MASSACHUSETTS INSTITUTE OF TECHNOLOGY

LINCOLN LABORATORY

RADIO-ECHO OBSERVATIONS OF THE MOON AT 3.6-CM WAVELENGTH

J. V. EVANS

Group 314

TECHNICAL REPORT NO. 256

19 FEBRUARY 1962

ABSTRACT

Radio-echo studies of the lunar surface in the wavelength range 3 meters to 10 cm indicate that the surface is smooth and undulating for the most part, with an average surface gradient of the order of one in ten. Photometric studies of the brightness distribution over the moon's disk, on the other hand, demonstrate the existence of microstructure which causes the surface to appear very rough at these much shorter wavelengths. This report describes radio-echo measurements of the reflection properties of the moon at a wavelength of 3.6 cm. The results show that the surface appears a good deal rougher at 3.6 cm than at meter wavelengths. Some 30 per cent of the reflected power is returned from scatterers that are uniformly distributed over the surface. The remainder is reflected from a region at the center of the visible disk which has a radius of about half the lunar radius. In this region, the surface appears to be describable by means of a Gaussian spatial autocorrelation function with a mean surface gradient of one in three.

LEXINGTON MASSACHUSETTS

RADIO-ECHO OBSERVATIONS OF THE MOON AT 3.6-CM WAVELENGTH

I. INTRODUCTION

Radio-echo observations of the moon have been made during the past decade at wavelengths that range between 3 meters and 3 centimeters. This work has been summarized and discussed both by Evans[1,2] and by Evans and Pettengill.[3] The principal results are that the lunar surface scatters radio waves in a distinctly different way from the manner in which it scatters light. At radio wavelengths most of the energy is reflected from a small region at the center of the visible disk, whereas at optical wavelengths (at full moon) the surface appears almost uniformly bright.[4]

Theoretical studies[5,6] of the scattering mechanism indicate that the radio observations may be interpreted as showing that the lunar surface is largely smooth (to the order of a few centimeters) and undulating, with average surface gradients of the order of one in ten. The autocorrelation function, which describes how the height of the true surface departs from a smooth sphere as a function of distance measured over the sphere, appears to be exponential in character and is certainly not Gaussian. Similar exponential autocorrelation functions have been found to describe many types of terrain on Earth.[7]

From photometric studies of the moon, Minnaert[8] concludes that the surface "is apparently an assembly of closely packed holes of all sizes superposed and juxtaposed, excavated in dark material." The way in which the surface reflects will be largely independent of the size of these holes, provided that their dimensions are much larger than those of the incident exploring wave. Thus the photometric studies of the moon yield information only about the microstructure of the surface (perhaps having a scale size measured in fractions of a millimeter), and the radio-echo observations are sensitive only to structures having scale sizes in the range many tens of wavelengths to some fraction (~0.25) of a wavelength.

Radar observations of the moon at a wavelength of 3 cm have been reported by Kobrin.[9] At the present time no measurements have been made at a shorter wavelength.* However, Kobrin employed a low-power CW bistatic radar, and was unable to determine the brightness distribution across the surface. The shortest wavelength at which the brightness distribution has been measured is 10 cm (Hughes[10]). Therefore, there is a considerable interval between the shortest wavelength at which radar observations have been made (and consequently the smallest structure size encountered) and the largest structure sizes examined (perhaps $\sim 10^{-2}$ cm) at optical wavelengths by means of photometric observations. Although it would seem doubtful that this gap in our knowledge will ever be completely removed by means of earth-based observations – in view of the strong atmospheric absorption at these intermediate wavelengths – the radio observations can be conducted at still shorter wavelengths than so far employed. As the wavelength is reduced,

* To the best knowledge of this author.

we should hope to find evidence that the moon becomes progressively rougher, tending toward the completely rough surface observed visually.

With this object in mind, radar observations of the moon were made at a wavelength of 3.6 cm, using the Camp Parks terminal (Pleasanton, California) of the Project West Ford Communications System. This report describes these observations and their reduction, and draws certain conclusions concerning the lunar surface.

II. EQUIPMENT

A. The Antenna

The radar equipment at Camp Parks operates at a frequency of 8350 Mcps (i.e., approximately 3.6-cm wavelength) and employs a 60-foot-diameter paraboloid for both transmitting and receiving. At this wavelength the beam has an angular diameter of 0.14°. A linearly polarized wave is transmitted and received by using a horn as the primary feed with a Cassegrainian optical system. The rotation of the plane of polarization introduced by the Faraday effect in the earth's ionosphere is, at all times, less than 2° and can be ignored.

The paraboloid is steered in azimuth and elevation either by means of manual controls or by means of a digital electronic control system whose input is a punched paper tape. The tape specifies the required position of the antenna at 1-minute intervals and the rates of motion to be followed between these intervals. It is normally prepared in such a manner that the telescope will never be called upon to reverse its direction of motion (over short intervals of time). Thus, in general, the axis of the telescope will lag somewhat behind the true position of the center of the moon. The extent of this error is determined by the quantization of the levels which specify the rates of angular motion and, in the worst case, can cause a displacement of the axis of the beam and the center of the moon of one-tenth beamwidth (0.014°). Such an error occurs only toward the end of a 1-minute interval when, by chance, the difference between the desired and applied rates of motion is at its maximum.

In view of the small angular extent of the antenna beam (0.14°) in comparison with the angular diameter of the moon (~ 0.5°), large corrections for the effect of the beam must be applied to the results in order to determine the brightness distribution across the moon. These corrections will be discussed fully later.

B. The Transmitter

The transmitter employed in these experiments radiates a coherent signal obtained by frequency multiplication from a crystal standard (operating at a frequency in the vicinity of 1 Mcps). The final amplifier is a klystron which has a nominal output of 25 kw CW, although in these experiments the peak output was only 12 kw. The klystron amplifier requires a drive signal of about 5 watts which is obtained from a traveling-wave-tube device. In order to minimize waveguide losses, the klystron amplifier is mounted in a room directly beneath the reflecting surface of the parabola, so that only about 10 feet of waveguide are required to conduct the transmitted energy to the primary feed. The feed horn projects through the reflecting surface and is directed toward the secondary mirror which is supported by a tripod. The high-voltage power supply for the klystron, the controls for the latter, the water cooling, magnet and heater supplies are all in the main building; hence, a large number of cables are required to connect the klystron to its supplies.

The transmitter is capable of radiating a continuous wave (and is then normally modulated by frequency-shift keying), but in these experiments it was pulse-modulated in the manner shown in Fig. 1. A 1-μsec pulse is applied to the "transmit" filter; this causes the filter to ring and produce a sinusoidal output whose frequency varies linearly with time between 0 and 90 kcps over a period of 300 μsec. This "chirp" is mixed with a local oscillator at 13 Mcps and the resulting signal passes through a filter designed to transmit only in the 13.06- to 13.09-Mcps range. Thus the RF drive is pulsed ON for a period of 300 μsec at a pulse repetition frequency (prf) of 20 cps. This prf is derived from the station master clock.

C. The Receiver

The frequency to which the receiver is tuned is maintained exactly equal to the transmitter frequency by employing, as local oscillators, the same crystal oscillators that were used to derive the transmitter signal. This arrangement is shown in Fig. 1. A traveling-wave maser is employed as first stage in the receiver, followed by a conventional crystal-diode mixer and preamplifier. The effective noise temperature of the maser-mixer system was measured to be approximately 40°K.

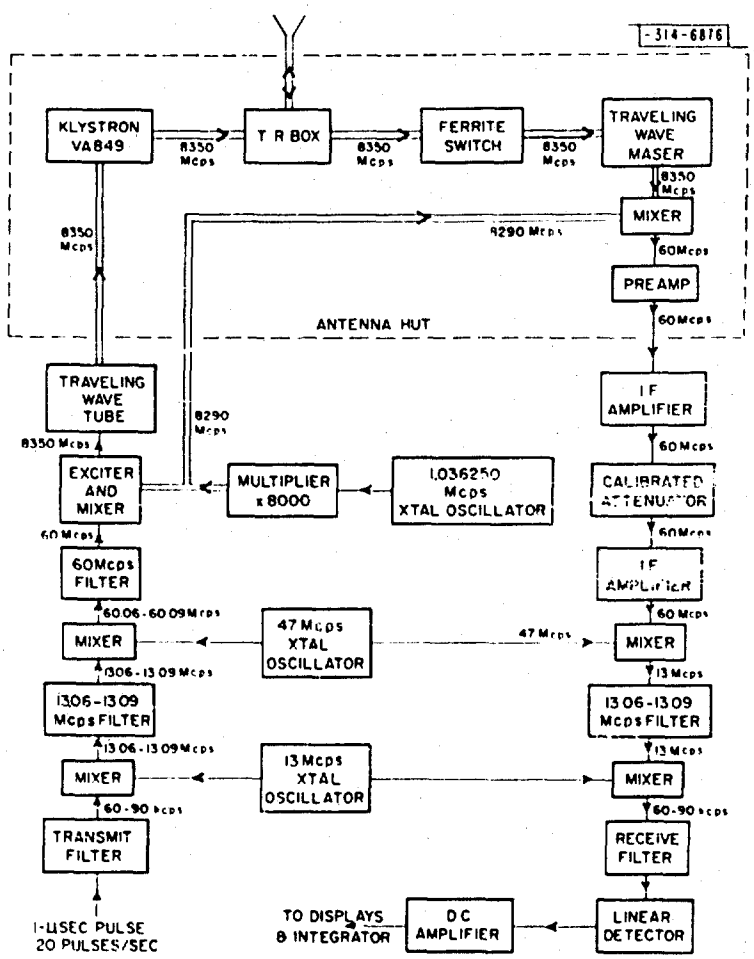

Fig. 1. The frequency control system of the Camp Parks (Project West Ford) radar.

To protect the maser from the strong signal put out by the transmitter, a combination of switches is used. The first switch is an electromechanical one and is indicated in Fig. 1 as the TR box. This device comprises a rotating disk which penetrates the waveguide between two 3-db couplers. The disk reflects the transmitter into a matched load during its OFF period and a hole in the disk connects the transmitter to the antenna during the ON period. The same disk reflects the antenna power into the receiver arm during the receive period. A further pair of 3-db couplers, together with a second disk, is placed in the receiver arm. Both disks are mounted on the same shaft and this is driven synchronously at 20 cps (the prf). This second pair of 3-db couplers and disk serves to connect the receiver to a matched load during transmit periods, and also reflects any power from the transmitter which has leaked through the first disk into a matched load. A large slot is cut in the second disk so that the receiver is connected to the antenna for most of the time.

The second switch is a conventional ferrite switch that operates by the Faraday rotation of the plane of polarization of the wave. The magnetic field for the switch is provided by a solenoid which is turned on during the required receive period. These protective devices introduce a large amount of unwanted attenuation between the feed horn and the maser, even though the latter (like the transmitter klystron) is mounted in the antenna hut. It was estimated at the time of these observations that the losses in the waveguide raised the effective receiver temperature by 60° to a total of 100°K. The sky temperature (together with "spill-over") raised the over-all system temperature to 120° ± 10°K. When the antenna was directed toward the moon, however, the over-all system temperature was higher by at least another 100°K.

There are no reliable reports of any variation of the brightness temperature of the moon with phase at this wavelength.[11] At present there is a wide variation in the published values of the lunar temperature, but it would appear that the temperature is of the order of 245° ± 20°K (Ref. 11). Hence it is concluded that, when the antenna is directed toward the center of the moon, the system temperature is 225° ± 20°K, assuming an antenna efficiency of 50 per cent.

For an echo reflected from a stationary point target, the output of the last mixer stage in the receiver will be a signal whose frequency varies linearly from 60 to 90 kcps over an interval of 300 μsec. A target which is extended in range may be considered as a succession of point targets, and hence gives rise to a complex reflected signal which is a superposition of many individual "chirps." The received "chirp" is applied to a "receive" filter whose impulse response is approximately the Fourier transform of that of the "transmit" filter. The "receive" filter, therefore, causes delays in the frequency components of the "chirp" which decrease with increasing frequency, thereby causing the 60-kcps component to be delayed the most. The pulse is therefore compressed, and the output of the filter is a pulse only 30 μsec long. The over-all system may be thought of as a 30-μsec pulsed radar that has an equivalent peak power ten times that actually radiated. In practice, small amounts of power are contained in subsidiary 30-μsec pulses that precede and follow the main one. The multipath properties of the moon can cause these "sidelobes" to interfere with the main pulse from a given range and degrade the performance of the radar. In this instance, all the "sidelobes" are about 20 db weaker than the main pulse and their presence has been neglected in this report. Finally, a linear (voltage) detector is employed at the output of the "receive" filter and the detected signal is both displayed and fed to an amplitude-vs-range integration system.

The design, construction and operation of the radar equipment described above was undertaken principally for Project West Ford, and at no time did this author contribute in any way to this effort.

D. The Integrator

Radar signals reflected from the moon are subject to deep fading as a consequence of the interference between the signals reflected from many independent scattering centers on the surface. The frequency of the fading is a function of (1) the apparent rate of libration of the moon, (2) the radar wavelength and (3) range measured from the leading edge of the moon. At a frequency of 8000 Mcps the fading is quite rapid, having a quasi-period of the order of 0.1 second.

In order to make precise measurements of the echo power as a function of range, it is necessary to average over many sweeps of the radar time base. This was accomplished in an analogue integrating system which employs a total of 36 integrators, each identical to that shown in Fig. 2. Each integrator is formed by a resistor R, a condenser C and a "chopper-stabilized" DC amplifier which jointly form a Miller circuit. The DC amplifier has a gain of approximately 10^8 and is carefully constructed so that, when used in conjunction with a low-leakage mylar condenser (C), a self-time-constant of the order of several hours is achieved. Since the integration was never continued for periods greater than 10 minutes, it is believed that the largest errors in the summation process arose from "drifts" rather than from leakage of stored energy.

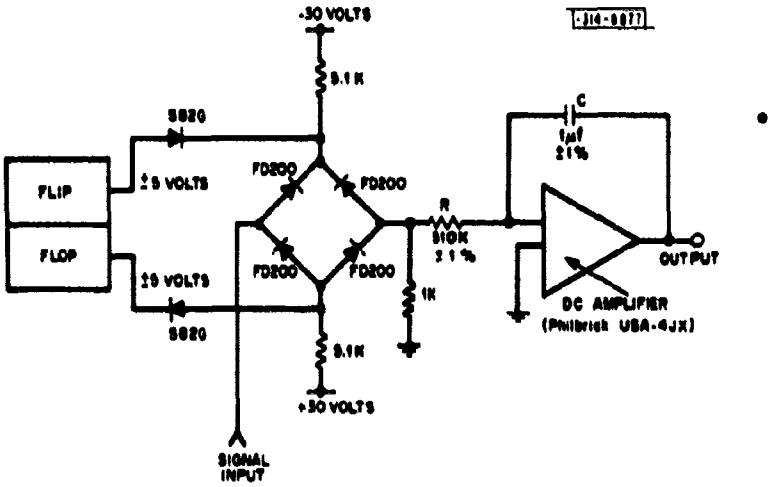

Fig. 2. The postdetector integrator circuit.

The signal to each Miller integrator is gated through a switch formed by four diodes in a bridge circuit (Fig. 2). The diodes are normally conducting because a 60-volt supply is applied to opposite ends of the bridge. This causes the input and output points of the bridge to be connected through the equivalent resistance of a single diode (~ 200 ohms). This resistance is small compared with R. During the time that the "switch" is closed, the output voltage e_o will increase according to

$$e_o = \frac{1}{RC} \int_o^t e_i \, dt \qquad (1)$$

where e_i is the input voltage applied to the bridge. The switch will be opened when the flip-flop shown in Fig. 2 changes to a state that causes the S82G diodes to conduct. In this case the resistance between the input and output points is approximately 10^9 ohms. A 1000-ohm resistor at the output of the bridge now effectively grounds the input to the Miller integrator, causing its output e_o to remain constant.

Error voltages occur as a result of DC potentials or drifts. The three main sources of these drifts are described in the following subsections.

1. DC Amplifier Drifts

The DC amplifiers are provided with balancing potentiometers, and these were normally adjusted to cause e_o to change at a rate of less than 1 mv/sec when the input to the integrator is grounded and R is reduced to 10,000 ohms. Thus, in normal operation, the unbalance in the DC amplifiers might be expected to cause a drift of 20 μv/sec, or a total drift of not more than 6 mv in a 5-minute period of integration. This could be reduced by increasing RC, but then e_o would decrease by the same amount and the signal-to-drift ratio would not be improved.

2. DC Unbalance of the Bridge When Conducting

The 60-volt power supply which causes the bridge to conduct is "floating" with respect to ground and, in the absence of a signal, the output of the bridge should be at ground potential. However, if the forward voltage drop across each diode in the bridge is not the same, the input and output potentials of the bridge will be different. Hence, if the input potential is at ground (via the output impedance of an amplifier), the output potential cannot be at ground, and an error signal will appear which will cause the integrator to drift. This problem was largely overcome by matching the diodes into groups of four which all exhibit approximately the same forward voltage drop. However, DC error voltages of the order of ± 2 mv still remain. These can be neglected if the rms signal is very large. Unfortunately the peak signal is limited to about 4 volts by the voltage applied by the flip-flop to the S82G diodes. Hence, for a narrow-band Gaussian noise input, an rms signal of ≤ 0.5 volt is the most that can be applied, and errors of the order of approximately 0.5 per cent can arise from the DC unbalances in the switches.

3. DC Unbalance of the Bridge When Nonconducting

When the gate is switched off, the potential at the output of the bridge may again differ from ground because the back impedance of the diodes, though very large ($\sim 10^9$ ohms), may be very unequal. In particular, when the integrator is used to examine short-range intervals (say 10 μsec) at a prf of 20 cps, the switch spends 5000 times longer in the OPEN than in the CLOSED position; hence, the DC offsets when OPEN must be correspondingly smaller to cause only about the same drift. This is achieved by grounding the output of the bridge via a 1000-ohm resistor. A lower value would be desirable, but the forward impedances of the bridges when conducting are not all identical, and hence the signal is attenuated by different amounts. With the present arrangement (1000-ohm resistors), this effect may introduce errors of the order of ± 0.1 per cent. Larger errors than this could not be tolerated.

The rms drift of the 36 integrators experienced in a 5-minute run is of the order of ± 12 mv and, in practice, the integrators drift in much the same fashion from run to run. The signal voltage e_o is directly proportional to the width of the range gate. For the experiments reported

here, a minimum width of 20 μsec was employed, for which e_o was typically 60 mv. Thus the drifts are, at worst, of the order of ± 20 per cent. By repeating the integration with no signal applied and subtracting the observed drifts, the uncertainty in e_o is reduced to approximately ± 2 per cent. For wider gate widths the error is correspondingly reduced, and is approximately 0.2 per cent for 200-μsec range intervals.

The flip-flops shown in Fig. 2 are connected to form a 36-stage shift-register delay line as shown in Fig. 3. This delay line is programmed to open and close the diode switches in sequence for equal intervals of time, thus causing the integrators to sum the energy corresponding to different range intervals along the time base. The digital equipment shown in Fig. 3 also enables fixed rates of range drift to be incorporated to match the motion of the echo along the time base (caused chiefly by the rotation of the earth). Fine adjustment of the position of the echo relative to that of the gate is provided by the delayed sweep controls of an oscilloscope.

The output voltages e_o are sampled in turn by a stepping switch, and then measured by a digital voltmeter. An electromechanical printer connected to the voltmeter prints the value of these voltages on a paper chart in the form of a list. The parameters of all the equipment are summarized in Table I.

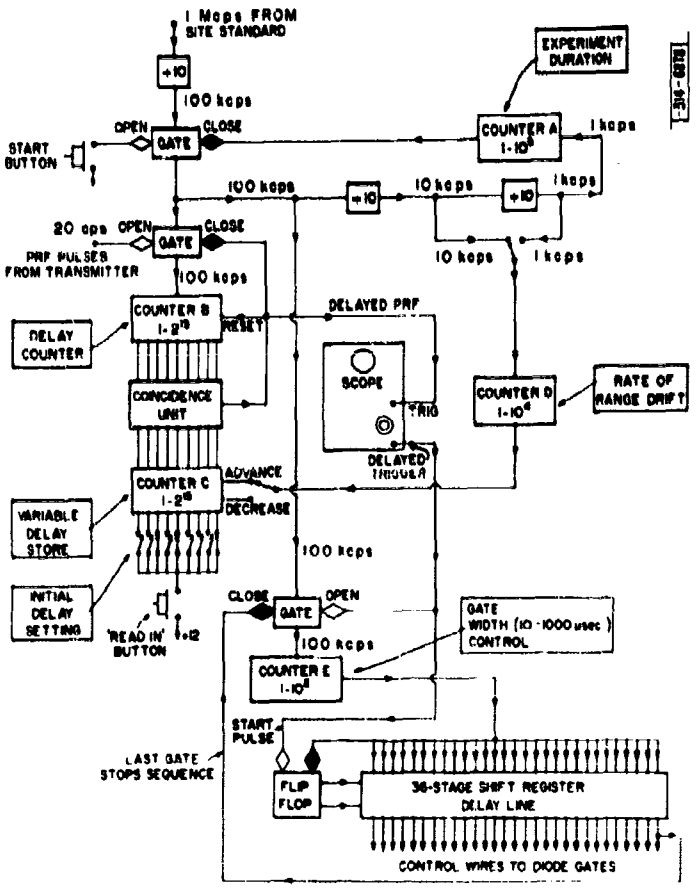

Fig. 3. Integrator digital control system.

TABLE I
SUMMARY OF EQUIPMENT PARAMETERS

Frequency	8350 Mcps
Antenna	60-foot paraboloid with Cassegrainian feed arrangement
Antenna gain	61 ± 1 db
Effective antenna aperture	150 ± 10 meters^2
Peak transmitted power	12 ± 1/2 kw
Pulse length	300 μsec
Pulse compression ratio	10:1
Over-all system temperature (when pointed at the moon)	225° ± 20°K
Receiver bandwidth	~30 kcps (i.e., matched to a 30-μsec pulse)
Over-all feeder losses	1.5 ± 0.2 db
Video integration	Generally 18 to 20 db

III. THE OBSERVATIONS AND THEIR REDUCTION

A. Introduction

Radio-echo observations of the moon are frequently made with the Camp Parks (Project West Ford) radar system, and the only special feature about the observations reported here is that the returns were integrated by using the equipment described in Sec. II-D. Observations were made on 6 - 9 and 11 September 1961. For the most part, the tracking of the moon was performed by the digital control system, although on some occasions manual tracking was attempted.

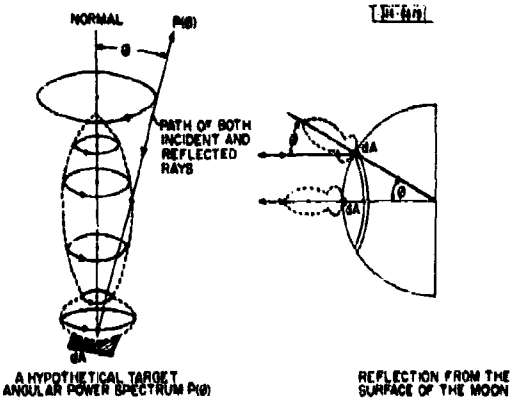

Fig. 4. The radar angular power spectrum $\bar{P}(\varphi)$.

The object of the experiment was to determine the function $\bar{P}(t)$ which describes how the echo power varies as a function of range delay measured from the leading edge of the moon. Because a given range delay t defines an annulus on the moon's surface, which is also defined by the angle φ between the ray path and the normal to the surface, the function $\bar{P}(t)$ can be transformed into a curve of reflected power vs the angle of incidence φ. This function $\bar{P}(\varphi)$, we shall call the target angular power spectrum. If it is assumed that the surface has the same kind of materials and the same kind of roughness everywhere, then the target angular power spectrum $\bar{P}(\varphi)$ can be regarded as the polar diagram (for backscattering) of any element on the surface. This is shown in Fig. 4 and the transformation from $\bar{P}(t)$ to $\bar{P}(\varphi)$ is simply a property of a spherical target which has been recognized by many workers (see Green[12]). There are other methods by which the target angular power spectrum $\bar{P}(\varphi)$ may be determined, and these have been described elsewhere.[13,14] The most impressive demonstration of the simplicity of the method outlined above has been provided by the work of Pettengill[15] who used a wavelength of 68 cm.

B. Method

In view of the narrow antenna beam employed in the experiment, it is evident that the function $\bar{P}(t)$ observed when the antenna is directed at the center of the moon will be the convolution of the true function for $\bar{P}(t)$ (i.e., the one that would be observed with a wide beam) with the antenna beam pattern. As a consequence of this, echoes could not be distinguished beyond a delay of 2 msec measured from the leading edge of the moon, although the full radar depth of the moon is 11.6 msec. Thus observations were also taken with the antenna beam directed away from the center of the moon, in order to observe echoes at greater ranges. The influence of the antenna pattern is different for each position of the beam, and hence the reduction of each set of observations will be discussed separately.

Considerable effort was made to obtain a truly linear detector law. In theory a square-law detector should have been employed, since the required function $\bar{P}(t)$ is the average of the sums of the powers reflected from different ranges, i.e.,

$$\bar{P}(t) \propto \sum P_{t_1} + P_{t_2} + P_{t_3} + \ldots + P_{t_i} \quad , \tag{2}$$

where i represents the i^{th} sweep of the time base and t is the range of interest. Unfortunately the dynamic range of the diode gate switches is small (0 to 4 volts) and, because the rms signal must be substantially larger than the unwanted DC offsets introduced by the switches (Sec. II-D), a linear detector is preferable to a square-law detector. Thus the voltages measured on the condensers represent the average amplitude $\bar{A}(t)$ of the echoes (and noise),

$$\bar{A}(t) \propto \sum A_{t_1} + A_{t_2} + A_{t_3} + \ldots + A_{t_i} \quad . \tag{3}$$

The echo amplitudes are known to have a Rayleigh distribution[1,16] and hence the echoes at any given delay resemble narrow-band Gaussian noise. It may be shown that, if such a signal having a standard deviation σ_s is applied to different detectors, the average output will be[17]

$$\text{Half-wave linear detector } \overline{A'} = \sqrt{\pi/2}\,\sigma_s \quad , \tag{4}$$

$$\text{Full-wave square-law detector } \bar{P} = 2\sigma_s^2 \quad . \tag{5}$$

A full-wave linear detector was employed in these observations and transmitted twice as much power as the half-wave detector. Hence we have

$$\text{Full-wave linear detector } \bar{A} = \sqrt{\pi}\,\sigma_s \quad . \tag{6}$$

Thus we see that $\bar{A}^2 = \pi\bar{P}/2$ and that, by squaring the average amplitude observed, the mean power may be obtained. The factor $\pi/2$ disappears in the analysis because only ratios of signal and noise powers are employed. Next we must consider the effect of the presence of the noise power. If the signal has (in the absence of noise) a standard deviation σ_s, and the noise (in the absence of signal) is σ_N, the observed standard deviation at the output of a linear detector will be proportional to $\sqrt{\sigma_s^2 + \sigma_N^2}$ because the signal and noise powers add before detection. It follows that, by squaring the average amplitude observed for signal and noise and subtracting the mean square amplitude of the noise alone, the mean echo power can be obtained. This procedure was followed in the reduction of the data. In practice it was not necessary to repeat the integration process with noise alone since there were always certain integrators which had summed only noise, and these could be averaged to determine σ_N^2.

The actual detector employed was linear for rms input voltages over the range 1 to 30 mv, i.e., over a range of 25 db. The peak signal-to-noise ratio was considerably in excess of this and hence observations were made with different levels of the signal into the detector to overcome this limited dynamic range. At high signal levels the gates closest to the peak of the echo would saturate, and their readings were ignored in the subsequent analysis.

C. Observations of the Central Region

Many measurements were made while tracking the center of the moon. The procedure generally adopted consisted of adjusting counter C (Fig. 3) to place the echo within the region covered by the gates, and then adjusting counter D to cause the gates to track the echo in range. Small

additional adjustments could be made by using the delayed sweep controls of the oscilloscope. Since ephemerides were not available to provide values for the rate of change in range, the adjustment of counter D could be accomplished only by trial and error. The basic timing of the digital circuits shown in Fig. 3 is 100 kcps; hence, the range tracking is accomplished by a series of 10-μsec "jumps." Accordingly the narrowest-range gate widths were employed only when the rate of range change was near zero (i.e., close to meridian transit). The motion of the moon relative to the earth was very close to its minimum value on 8 September 1961, and hence two 10-minute runs were made – one before and one after meridian transit – to obtain the distribution of echo power near the leading edge of the moon.* A similar pair of runs was made on 11 September, but on this occasion the antenna was steered manually (using a table of prediction positions) and the over-all tracking accuracy was inferior to that provided by the digital control system. These two sets of data are shown in Fig. 5. It can be seen that the peak observed on 11 September is distinctly more rounded than that observed on 8 September. This is attributed to the less accurate positioning of the antenna on that day, and all data taken with the antenna under manual control have been discarded. The convolution of the transmitter pulse (Fig. 6) with a step function is also shown in Fig. 5. It can be seen that the observed echo rises almost as fast as the step function. In view of the fact that the leading edge of the moon probably has an infinite impulse response resembling a step followed immediately by an exponential decay, good agreement between the two sets of points cannot be expected. Nevertheless the results indicate that, to the accuracy of these measurements (~ ± 10 μsec), the infinite impulse response of the leading edge of the moon is indistinguishable from a step.

The results shown for 8 September in Fig. 5 have been combined with other data obtained at two different signal levels, and gate widths of 100 μsec in Fig. 7. No echoes can be seen beyond 2 msec from the leading edge of the moon. The maximum mean signal-to-noise ratio observed at the leading edge of the echo is +26 db, and the signal-to-noise ratio is down to about +3 db at 1-msec range. The full-line curve of Fig. 7 has been drawn in by eye. The useful bandwidth of the Project West Ford communications equipment, using the moon as a reflector, is determined by the square of the Fourier cosine transform of this function.[18†]

In order to correct the results shown in Fig. 7 for the effects of the antenna pattern, a contour diagram of the radiation pattern was obtained from Mr. L. Niro of Group 315, and this is shown in Fig. 8. Mr. Niro obtained this pattern by making measurements of the signals radiated by a test transmitter which was placed some distance (on Mount Diablo) from the antenna for this purpose. Such a transmitter provides a convenient stationary target of high signal intensity. However, the effects of ground reflections may be serious, and the pattern observed when the antenna is close to 0° elevation may be considerably different from what it is at higher elevations, because of the changing gravitational load on the structure. Thus the pattern shown in Fig. 8 may not represent the true pattern experienced in these observations, but so far radio-star observations have not been made with sufficient precision to check Fig. 8 in great detail.

An "average" polar diagram was obtained from Fig. 8 in two ways. In the first method, polar diagrams were drawn for the projections a-a', b-b', c-c' and d-d'. These are shown in Fig. 9(a-b).

* During a 10-minute interval before or after transit, the earth's motion will introduce a range change of the order of 5 μsec.

† The effective single-channel bandwidth of the Project West Ford Communications System is discussed in Appendix A.

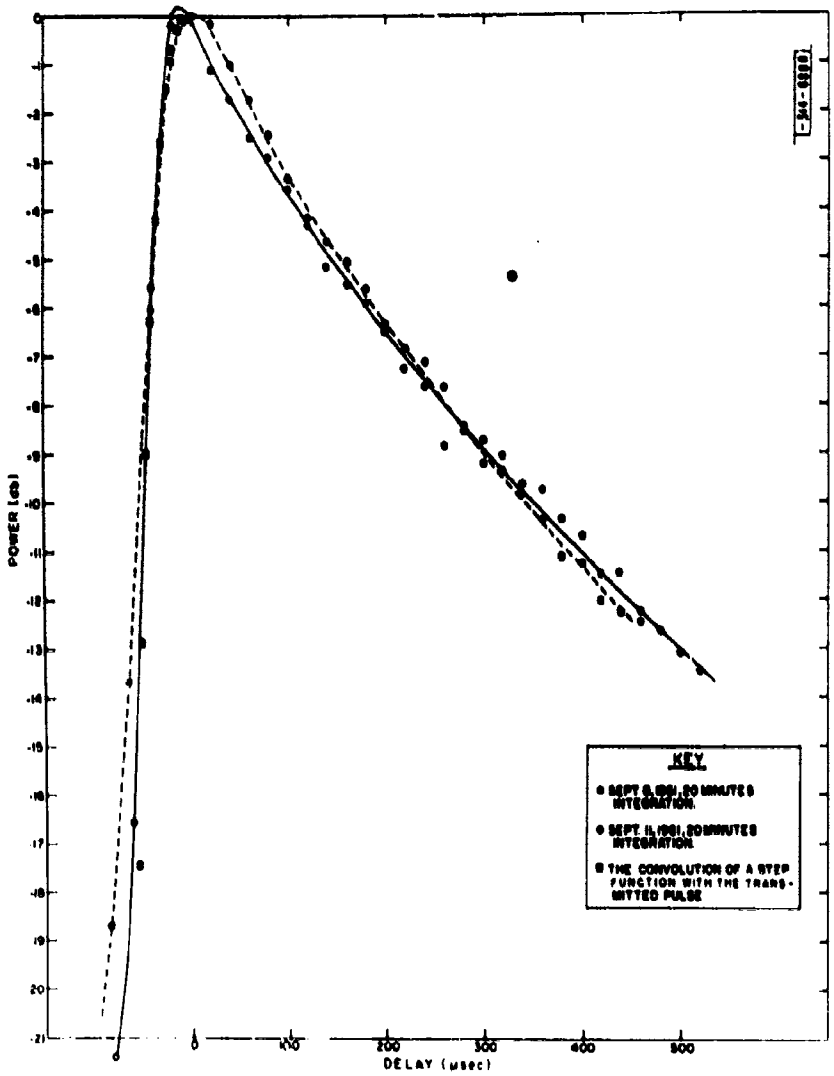

Fig. 5. Echo power vs range delay measured at 20-μsec intervals on 8 and 11 September 1961 (observations made at 3.6-cm wavelength). Also shown is the convolution of a step function with the pulse response of the equipment (Fig. 6).

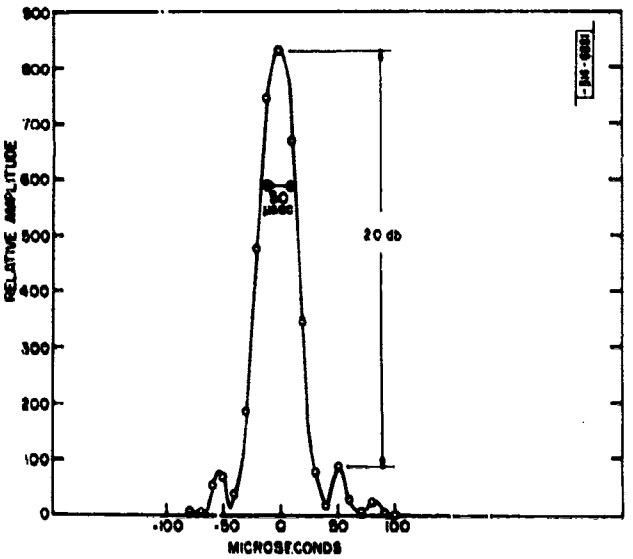

Fig. 6. The pulse response of the equipment. This diagram represents the output of the receiver integrated over 10-μsec delay intervals, when the transmitter pulse (suitably attenuated) was introduced into the receiver.

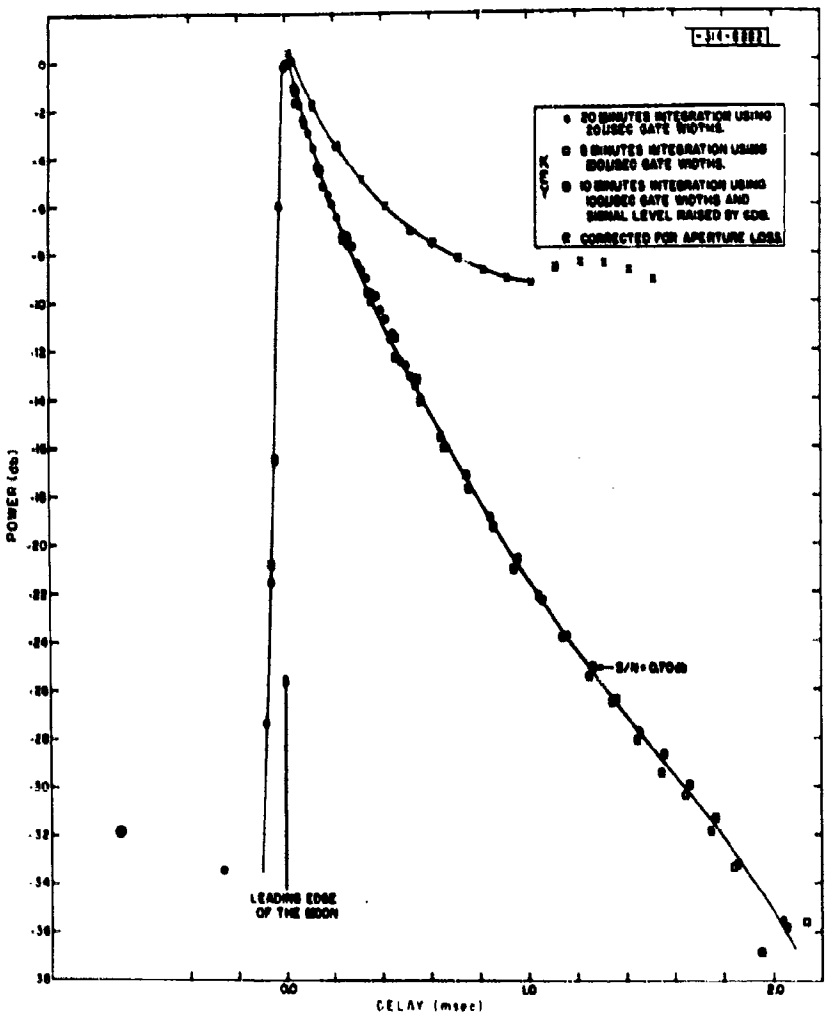

Fig. 7. The echo power as a function of range delay observed (at 3.6-cm wavelength) when the antenna was directed at the center of the moon. The crosses represent the curve of echo power vs delay obtained when the line through the experimental points is corrected for the effect of the antenna (Fig. 13).

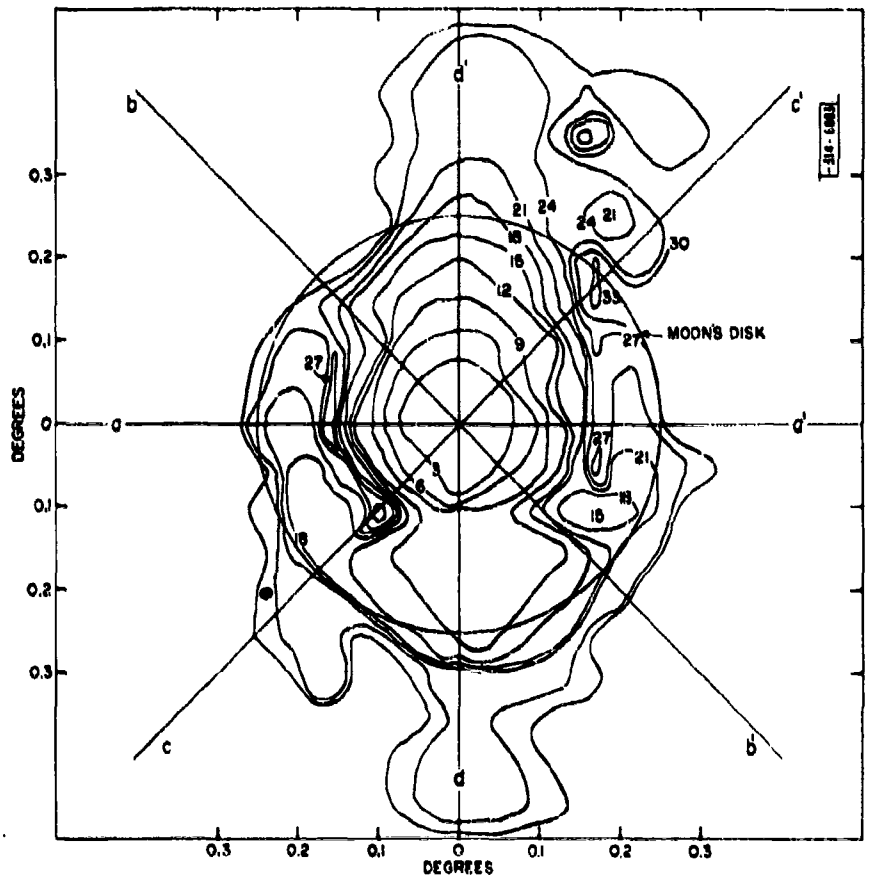

Fig. 8. The antenna contour diagram of the Camp Parks antenna. The intensity contours in this diagram are in 3-db intervals and indicate the manner in which the transmitter power is distributed across the moon's disk.

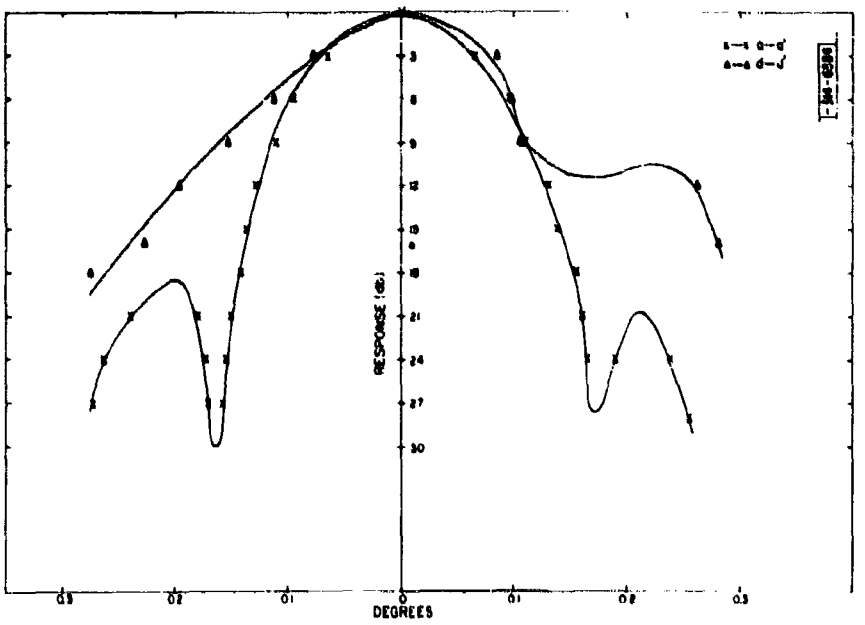

(a) For sections a-a' and d-d' shown in Fig. 8.

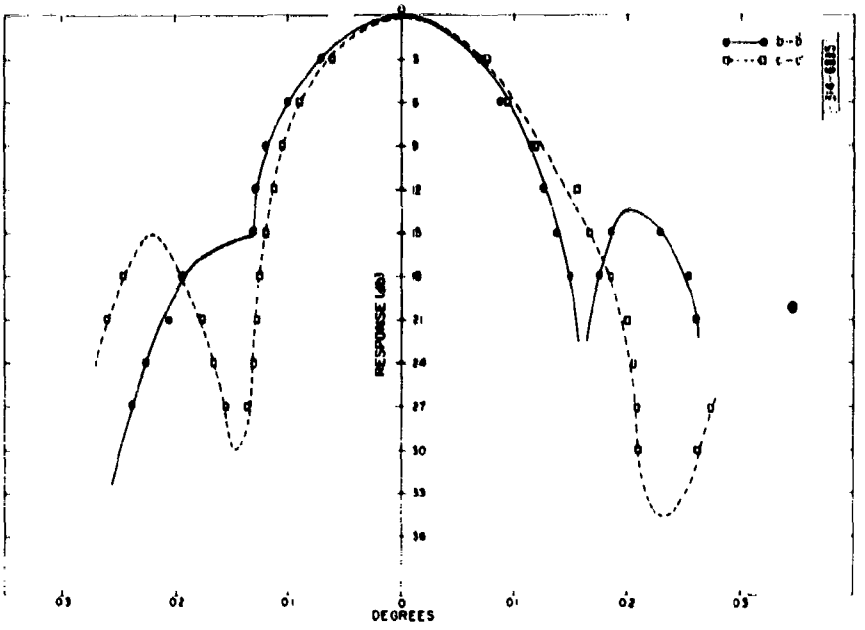

(b) For sections b-b' and c-c' shown in Fig. 8.

Fig. 9(a-b). The directional diagram for the Camp Parks antenna.

In all cases the half-power bandwidth is close to its theoretical value of 0.14°, but the behavior of the patterns beyond this point differs considerably. An "average" pattern was next constructed by taking the mean of all the curves of Fig. 9(a-b). This is shown as the broken line of Fig. 10. The alternative method was to measure the area (in square degrees) inside each of the intensity contour lines of Fig. 8 by planimeter and to equate this to the area of an equivalent disk in order to find the mean radius of the beam at this point. This method gave the full line of Fig. 10. The two curves agree well out to 0.10° and then differ, because the first method underestimates the importance of the large sidelobe below the main beam shown in Fig. 8. It was decided to adopt the full-line curve (in view of some evidence presented later) but not to attempt corrections beyond a 0.125° subtended angle. Because, in radar observations, the antenna pattern controls both the transmission and reception of the energy, the correction factors are the square of those shown in Fig. 10. The response curve finally adopted is shown in Fig. 11. This figure was then transformed into a diagram of the antenna correction as a function of range delay (Fig. 12) by means of a diagram which shows the half-angle subtended at the earth by annuli at different delays on the moon (Fig. 13). As can be seen in Fig. 12, the antenna corrections become very large (20 db) at a delay of only 1.5 msec. Hence the results (shown in Fig. 7) were corrected only out to this value. The corrected points were expected to show a monotonic decrease in power as a function of delay, and not increase, after a certain point as those shown in Fig. 7. It is presumed that the antenna corrections for a delay greater than 1 msec (0.10° subtended angle) are unreliable and hence the points beyond this value shown in Fig. 7 were subsequently ignored.

D. Observations at One Beamwidth Off-Center

The angle subtended by the lunar radius is approximately equal to two antenna beamwidths. Measurements were therefore made with the antenna directed off-center by one beamwidth (0.14°). Precise movement of the antenna relative to a median tracking path (provided by the digital control system) was permitted by means of manual controls. With the aid of these controls the antenna was directed 0.14° off in azimuth (right and left) and then in elevation (high and low). Five minutes' integration was performed in all four positions, using 500-μsec-wide range gates. Some of the positions were repeated to ensure consistent results. In all four positions of the antenna, the echo amplitude was reduced to a maximum mean amplitude of about +6 db, which occurred at a delay of 2 msec. These observations are shown in Figs. 14 and 15. Figure 14 shows that the results for the two azimuth offset positions agree quite well over the 2.5- to 7-msec range, but not in the 0- to 2.5-msec region. Thus it appears that this delay interval (0 to 2.5 msec) is illuminated largely by the sidelobes which are not symmetrical. Similarly the presence of the marked elevation sidelobes (Fig. 8) can be recognized by the strong echoes over the 0- to 2.5-msec range in Fig. 15, as distinct from Fig. 14. It was on this evidence that the full line of Fig. 10 was selected in preference to the broken one (Sec. III-C). It is further believed that any differences in the echo intensities observed in these four positions of the antenna are attributable to the asymmetry of the radiation pattern, rather than to distinct differences in the scattering behavior of the moon. Because of the absence of strong sidelobes along the azimuth axis (Fig. 8), the data presented in Fig. 15 were chosen for analysis. An antenna correction curve was obtained in the following way. A diagram was prepared which showed the range delay contours of the moon to scale (Fig. 16). A set of intensity contours, representing the idealized two-way antenna pattern (Fig. 12), was superimposed on the range delay contours. The intensity along each arc of a given delay contour is thus shown in Fig. 16, and the average intensity along a given contour is easily

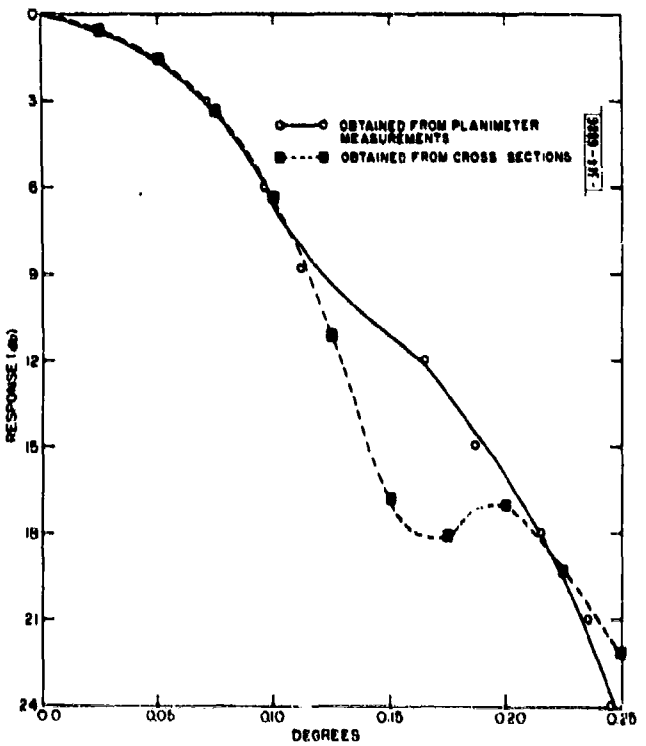

Fig. 10. The "average" directional diagram for the Camp Parks antenna obtained from (a) a mean of the curves shown in Fig. 9(a-b) (dotted curve) and (b) from planimeter measurements of the area inside each of the contour lines shown in Fig. 8 (full-line curve).

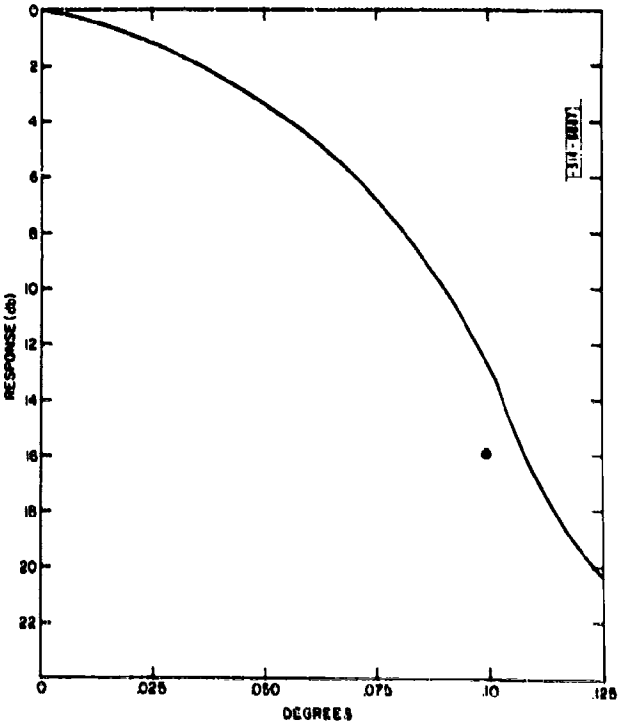

Fig. 11. The directional diagram for radar observations adopted for the Camp Parks antenna.

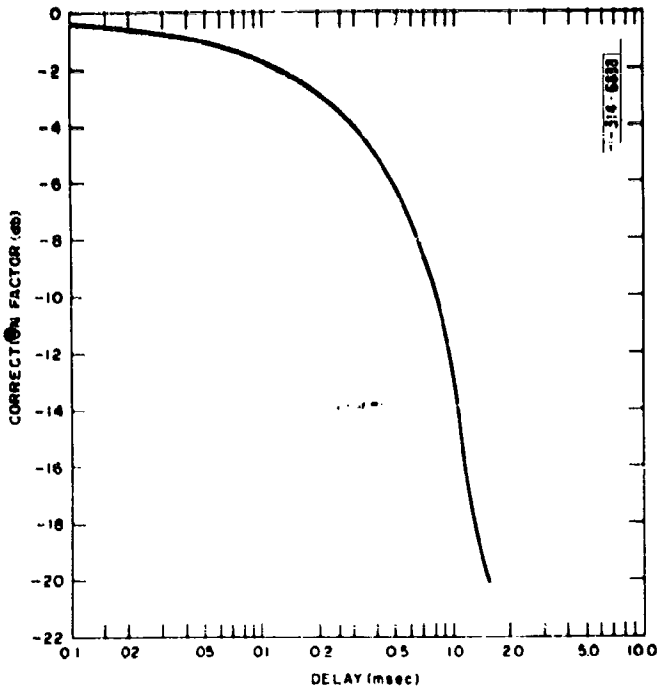

Fig. 12. The antenna correction factor shown in Fig. 11 is plotted here as a function of range delay. The conversion of coordinates was performed by using Fig. 13.

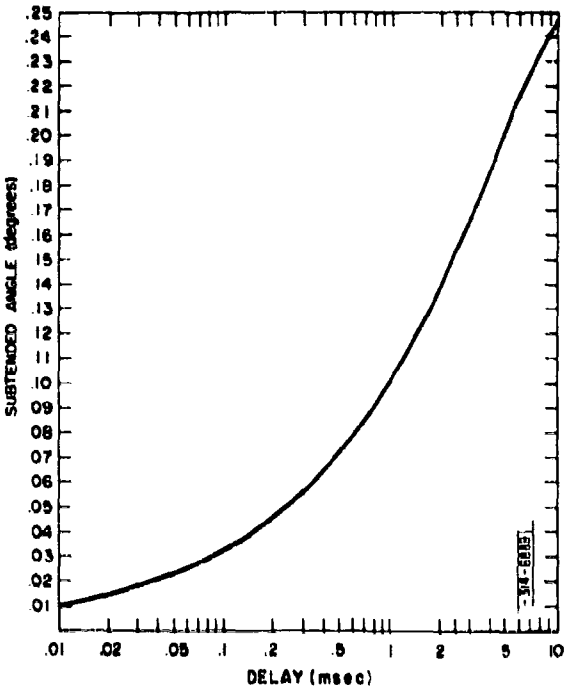

Fig. 13. The angle subtended at the earth between the center of the moon and another point on the moon's surface at a known radar delay time from the center. (This diagram was drawn for 11 September 1961 when the half-angle subtended by the moon's disk was 0.248°.)

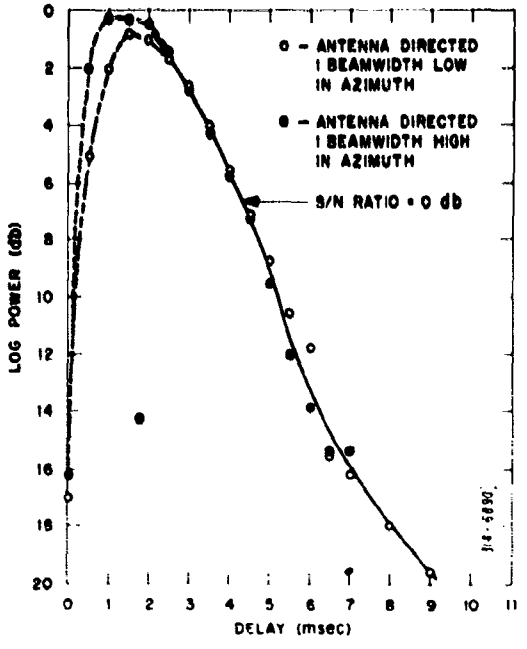

Fig. 14. Echo intensity with antenna offset in azimuth by one beamwidth.

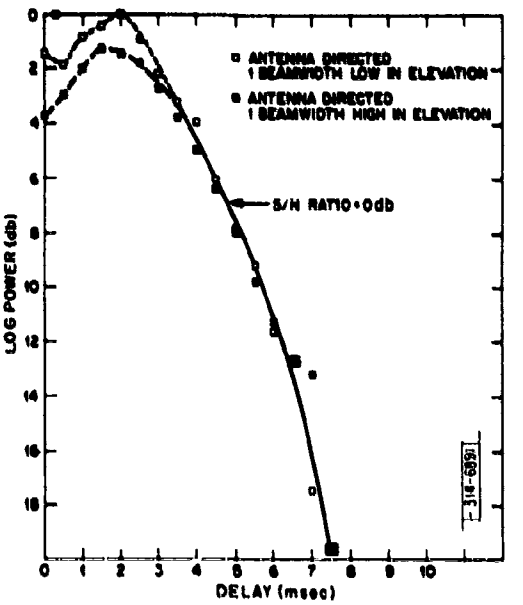

Fig. 15. Echo intensity with antenna offset in elevation by one beamwidth.

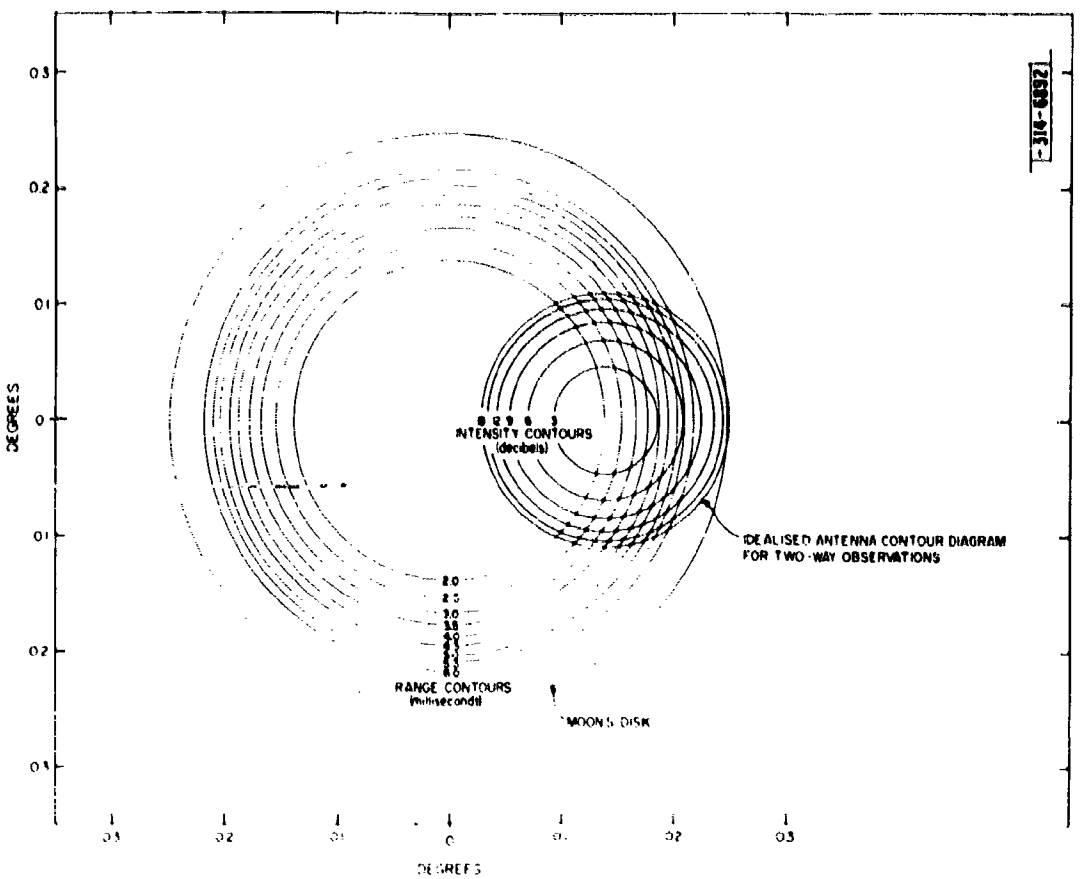

Fig. 16. This diagram shows, in plan form, the intersection of the range delay contours and the idealized antenna contour diagram when the antenna was directed one beamwidth (0.14°) from the center of the moon. Because the echo intensity is proportional to the projected area of the surface inside each contour line, it is possible to compute a new antenna correction diagram (Fig. 17).

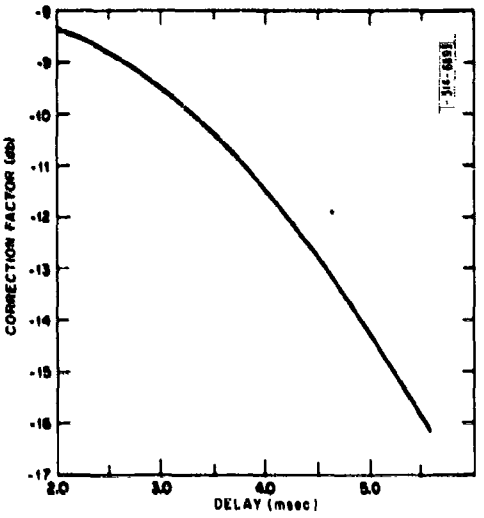

Fig. 17. The correction factor for the effect of the antenna pattern when the axis of the beam is displaced from the center of the moon by one beamwidth (0.16°).

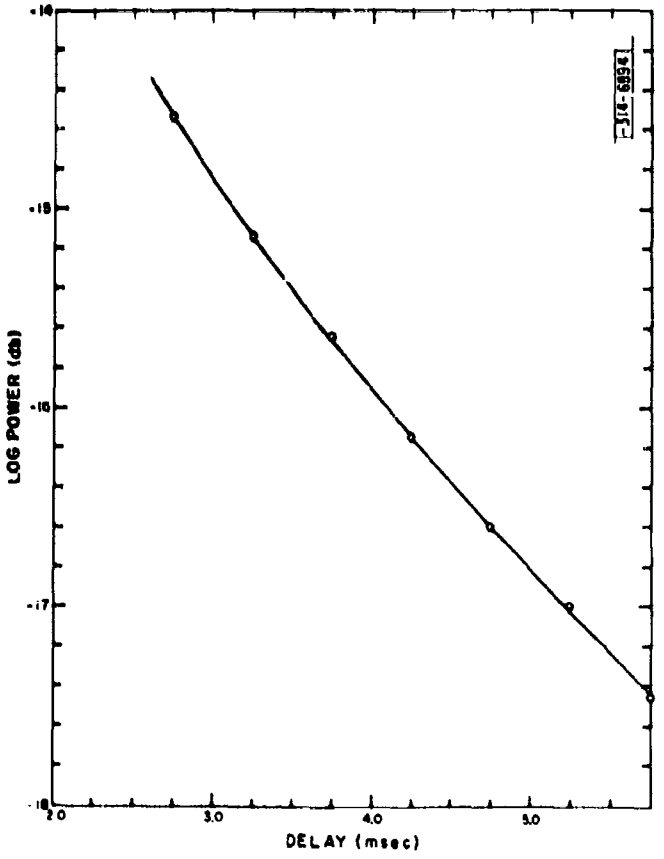

Fig. 18. The corrected values for the echo intensity (relative to zero delay) as a function of range delay obtained from the results shown in Fig. 14.

obtained by measuring the angle subtended by each arc at the center of the moon, weighting the angles according to the intensity contour in which they lie, and then summing. The antenna correction diagram obtained in this way is shown in Fig. 17 and the results of Fig. 14 when corrected are shown in Fig. 18.

E. Observations at One-and-a-Half Beamwidths Off-Center

When the beam was displaced by about one-and-a-half beamwidths, the axis of the beam was directed toward the limb of the moon. It was hoped that such a displacement would enable echoes up to 11.6 msec in range to be obtained. In the same manner as described in the preceding section, observations were made in all four quadrants, but this time with a displacement of 0.22°. Again the data obtained for azimuth displacements were chosen for analysis. These are shown in Fig. 19 where it can be seen that the maximum mean echo amplitude is now only ~0 db. Good agreement between the two sets of points exists over the 5- to 9.5-msec range.

A new antenna correction diagram (Fig. 20) was prepared in the manner outlined above, using the plane projection of the range and intensity contours shown in Fig. 21. The corrected values for power as a function of delay are shown in Fig. 22.

IV. TOTAL REFLECTED POWER

The results for the different time-delay intervals given in Figs. 5, 18 and 22 have been combined on a log-power vs log-delay plot in Fig. 23, and a smooth curve drawn through the points. When this smooth curve is replotted against a linear range-delay axis, Fig. 24 is obtained. The figure also shows the function for $\bar{P}(t)$ observed by Pettengill[15] with a wavelength of 68 cm and a pulse length of 65 μsec. Despite the obvious similarity between curves, it is immediately apparent that the "bright spot" at the center of the moon is less bright at 3.6 than at 68 cm.

Pettengill reports that the integrated power under the curve for $\bar{P}(t)$ observed at 68 cm yields a total cross section for the moon close to $0.074\pi a^2$, where πa^2 is the cross section of the projected disk. The value $0.074\pi a^2$ is that obtained by Fricker, et al.,[19] from a series of careful measurements made with a CW radar at a wavelength of 73 cm. It is also close to the mean value ($0.081\pi a^2$) of all the long pulse or CW measurements made in the wavelength range 3.0 meters to 33 cm (Ref. 2).

We may therefore take Pettengill's measurements as representative of the meter wavelength observations in order to compare the results presented here. The relative performance of the two radar systems is shown in Table II and a comparison of the echo intensities is given in Table III.

The uncertainty in the over-all performance of the Camp Parks radar due to imperfect knowledge of the equipment parameters is about ± 2 db. There is a similar uncertainty in the performance of the Millstone Hill radar, and thus a comparison of their relative performances is subject to an uncertainty of about ± 3 db. Thus Table II shows that the Camp Parks radar system is ~5 ± 3 db more sensitive than the Millstone Hill system. Despite this, the echo intensities observed at 5-msec delay indicate that the echoes at 68 cm were 2 db stronger than those at 3.6 cm (Table III), whereas the echoes from the leading edge of the moon differ by about 10 db. This difference represents the change in brightness at the leading edge of the moon only approximately, since the pulse lengths employed in the two experiments were not the same.

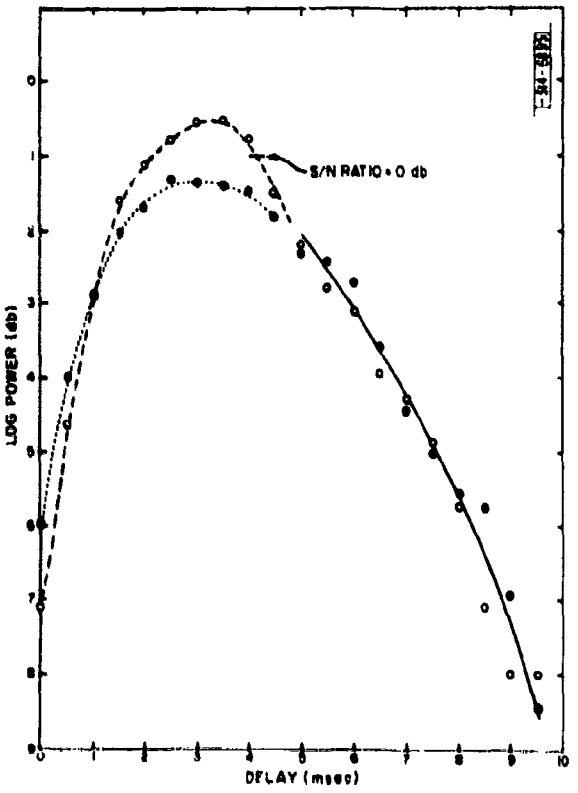

Fig. 19. The echo power vs range delay when the antenna was directed in azimuth 0.22° away from the center of the moon.

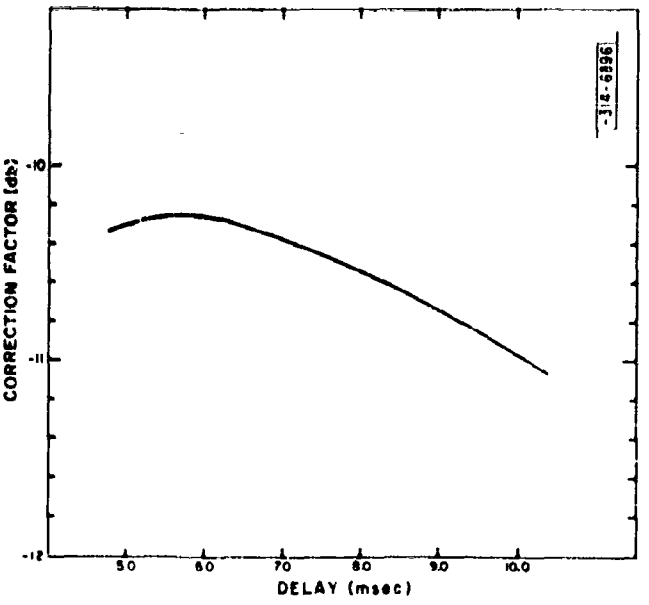

Fig. 20. The antenna correction diagram for the position of the beam shown in Fig. 21.

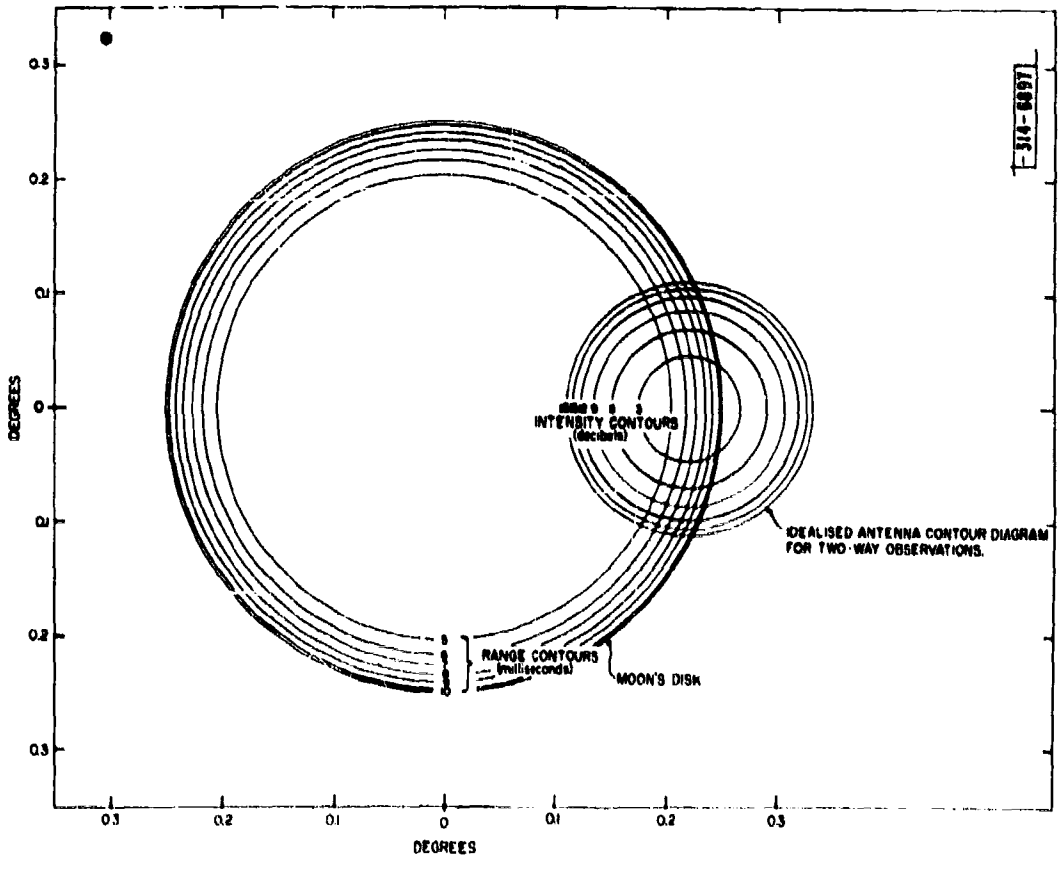

Fig. 21. This diagram shows the range delay contours and the idealized antenna contour diagram for observations conducted with the antenna beam directed 0.22° from the center of the moon's disk (i.e., approximately at the limb of the moon).

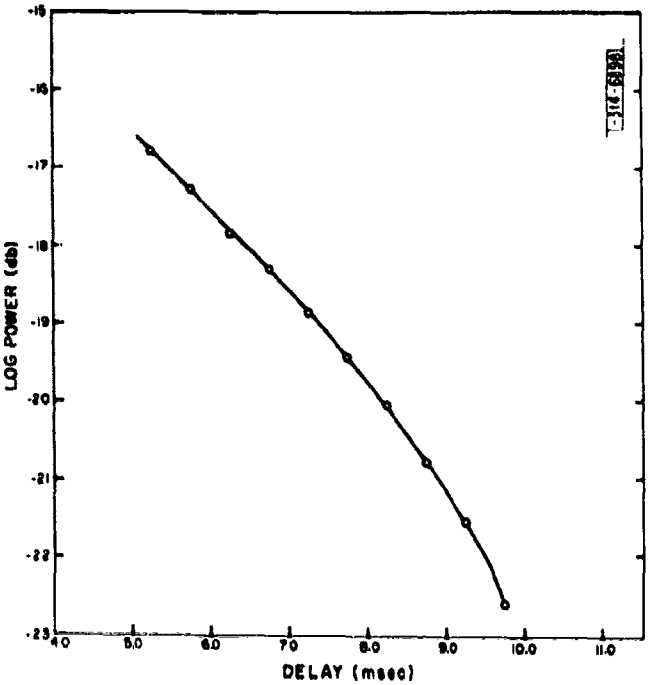

Fig. 22. Echo intensity vs range delay obtained by correcting the curve shown in Fig. 19 for the effects of the antenna (Fig. 20).

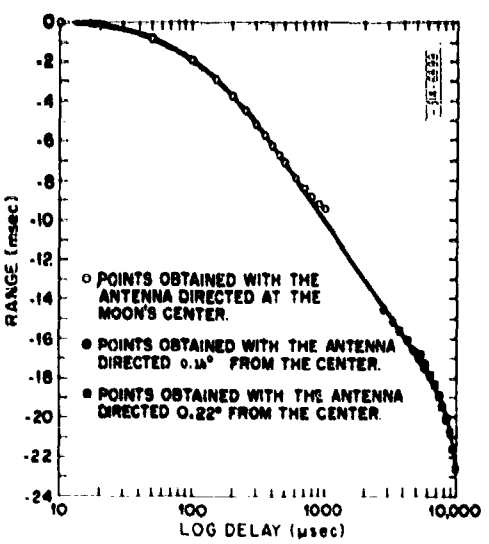

Fig. 23. Echo intensity vs log range delay. This diagram combines the results shown in Figs. 5, 18 and 22.

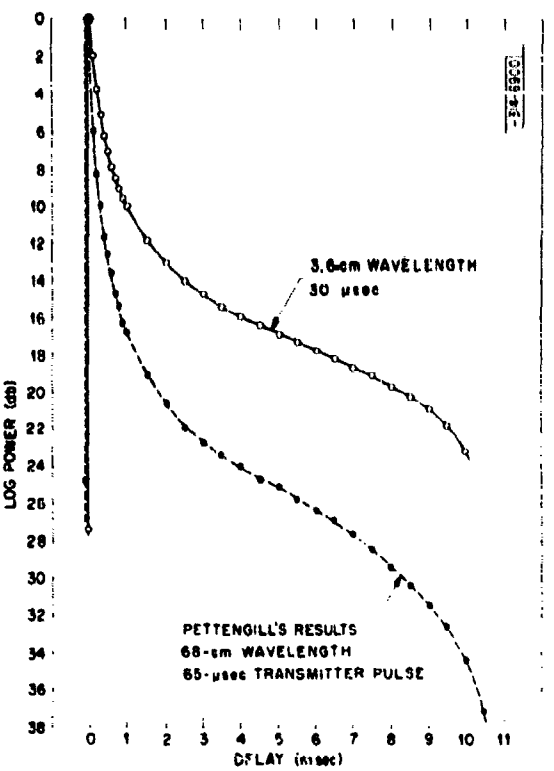

Fig. 24. The curve for echo intensity shown in Fig. 23 is plotted here against a linear range-delay axis. Also shown is the curve observed by Pettengill (Ref. 15) at a 68-cm wavelength.

TABLE II

COMPARISON OF MILLSTONE HILL AND CAMP PARKS RADAR SYSTEMS

Parameter	Millstone Hill	Camp Parks	Camp Parks vs Millstone Hill
Peak transmitted power	2.5 Mw	120 kw (effective)	−13 db
Antenna gain	38 db	61 db	+23 db
Antenna aperture	250 m^2	150 m^2	−2.3 db
Feeder losses	2 db	1.5 db	+0.5 db
Noise temperature (T)	245°K	225°K	–
Receiver bandwidth (b)	≈35 kcps	35 kcps	–
(kTb)	(−130 dbm)	(−130 dbm)	–
Pulse length	65 μsec	30 μsec	−3.0 db*
Sensitivity of Camp Parks vs Millstone Hill = +5.2 db			

* True only where $\bar{P}(t)$ does not vary rapidly with time (t).

TABLE III

COMPARISON OF ECHO INTENSITY AT 68- AND 3.6-CM WAVELENGTH

Parameter	Millstone Hill	Camp Parks	Camp Parks vs Millstone Hill
Signal-to-noise ratio of specular* peak	+31.3 db	+26.0 db	−5.3 db
Signal-to-noise ratio at 5-msec range	+6.2 db	+9.2 db	+3.0 db

When the equipment performance (Table II) is considered, the following ratios are obtained:
Specular* component at $\lambda = 68$ cm to $\lambda = 3.6$ cm = +10.5 db,
Rough* component at $\lambda = 68$ cm to $\lambda = 3.6$ cm = +2.2 db.

* The reasons for this classification are discussed later in the text.

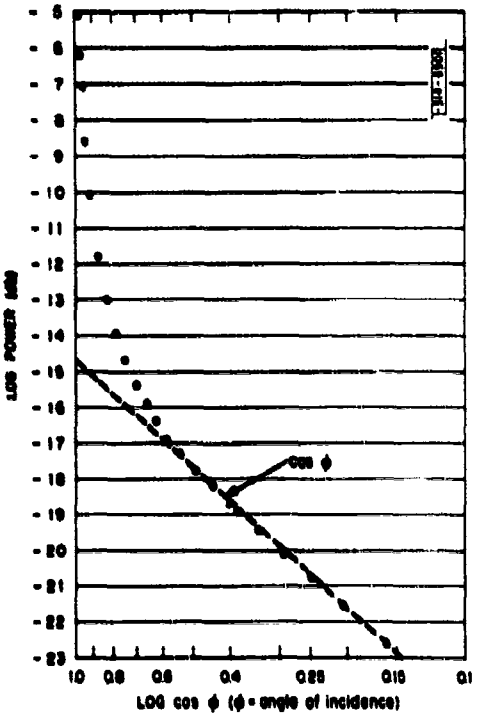

Fig. 25. Echo intensity plotted as a function of log cosϕ where ϕ is the angle of incidence and reflection of the ray. The power in the region $55° < \phi < 90°$ varies as cosϕ, indicating that the limb region of the moon appears to scatter isotropically at this wavelength (3.6 cm).

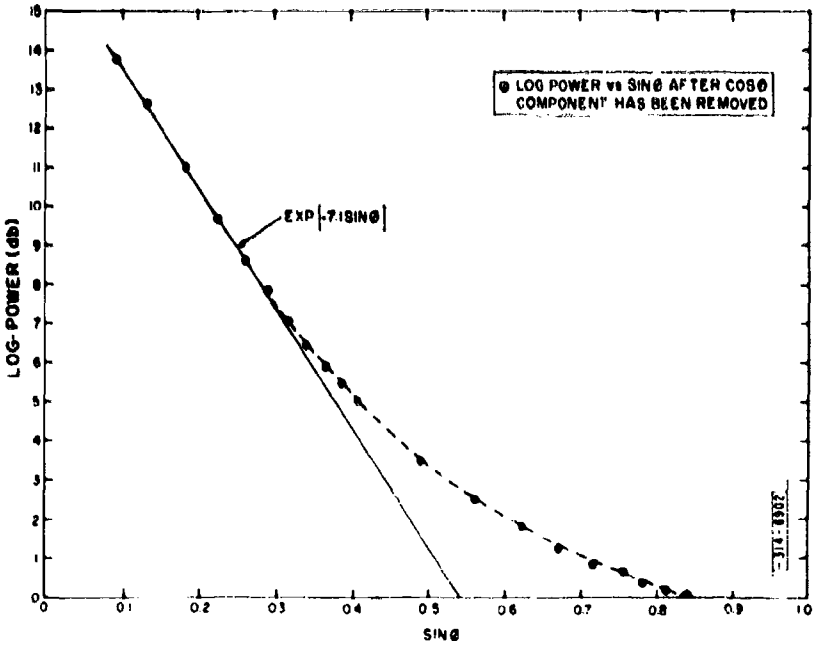

Fig. 26. The power in the "specular" component plotted as a function of sinϕ. In the region $5° < \phi < 18°$, the law $P(\phi) \propto \exp[-7.1 \sin\phi]$ is obeyed.

The echo power integrated under the curve of Fig. 23 yields a cross section of $\sigma = 0.02\pi a^2$. The uncertainty in this measurement is at least ±50 per cent and is in conflict with the value observed by Kobrin at 3 cm, which this author believes should have been stated $\sigma = 0.09\pi a^2$ with an estimated error of ±30 per cent (Ref. 2). However, Hughes[10] reports a value $\sigma = 0.021\pi a^2$ (±50 per cent) at a wavelength of 10 cm, and workers at the Jet Propulsion Laboratory[20] report a value $\sigma = 0.022\pi a^2$ ($^{+100\text{ per cent}}_{-50\text{ per cent}}$) for a wavelength of 12.5 cm. Therefore, it is possible that the reflection coefficient of the lunar surface may be substantially lower at these centimeter wavelengths than at meter wavelengths. Such a change could come about if the uppermost layer of the surface were more porous than that some small distance (~ 1 cm) below.

V. THE ANGULAR POWER SPECTRUM

The absolute level of the total echo power may be subject to unknown systematic errors. However, the angular power spectrum $\bar{P}(\varphi)$ depends only on the shape of the $\bar{P}(t)$ function, which need not be similarly in error. Pettengill[15] has shown that his results may be interpreted as indicating two distinctly different types of scatter on the surface. One component (the "rough" component) obeys the law

$$\bar{P}(\varphi) \propto \cos^{3/2}\varphi \quad , \tag{7}$$

and is responsible for the echoes observed at all range delays beyond about 2 msec. When this component has been removed, the remainder (termed the "specular" component) is found to obey the law

$$\bar{P}(\varphi) \propto \exp[-10.5 \sin\varphi] \quad . \tag{8}$$

The results presented in Fig. 24 have been plotted against the function log cos φ in Fig. 25. It can be seen that, over the range $55° < \varphi < 90°$, the law

$$\bar{P}(\varphi) \propto \cos\varphi \tag{9}$$

fits these observations extremely well. This law indicates that the limb region is uniformly bright, since the projected area decreases with range as cos φ. If this "rough" component is subtracted from the total power (Fig. 24) we should expect, by analogy with Pettengill's and Hughes' results, to be left with a specular component which would fit some simple law of the form

$$\bar{P}(\varphi) \propto \exp[-A \sin\varphi] \quad . \tag{10}$$

The remainder has therefore been plotted against sin φ in Fig. 26. It can be seen that the function $\exp[-7.1 \sin\varphi]$ fits the results near the origin ($5° < \varphi < 18°$) but not elsewhere. A search was therefore conducted for some other simple function which would fit the results. Of the many empirical laws tried, only the function

$$\bar{P}(\varphi) \propto \sin^{-1.75}\varphi \tag{11}$$

came near to fitting the results over the whole range of angles (Fig. 27). The theoretical form of the angular power spectrum for reflections from a plane surface having a number of facets oriented with a Gaussian distribution of angles to the normal has been shown[21,22] to be

$$P(\varphi) \propto \exp\left[-\frac{\tan^2\varphi}{2\varphi_o^2}\right] \quad . \tag{12}$$

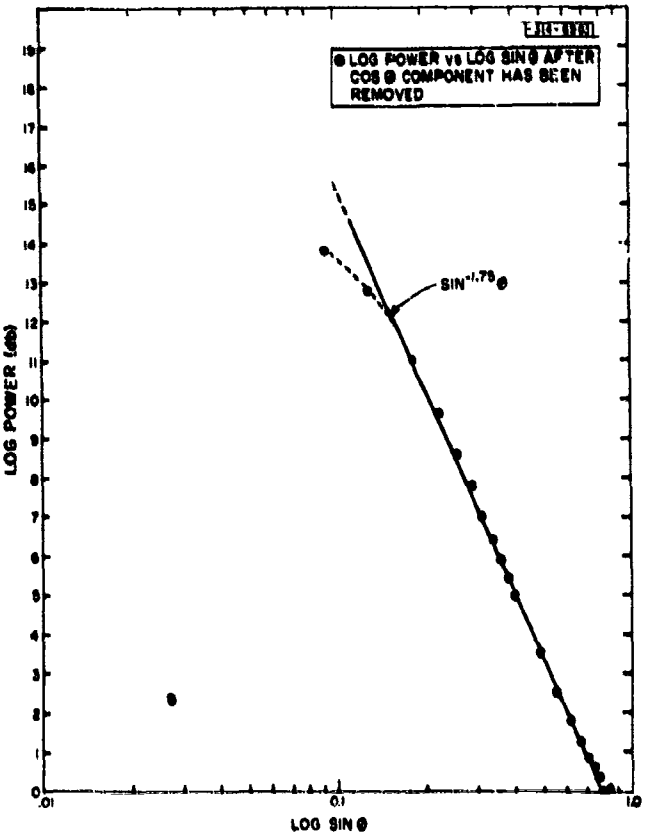

Fig. 27. The "specular" component plotted as a function of log sinϕ. The law $P(\phi) \propto \sin^{1.75}\phi$ was the only empirical law which could be found to fit the observed points over a substantial range of values for ϕ.

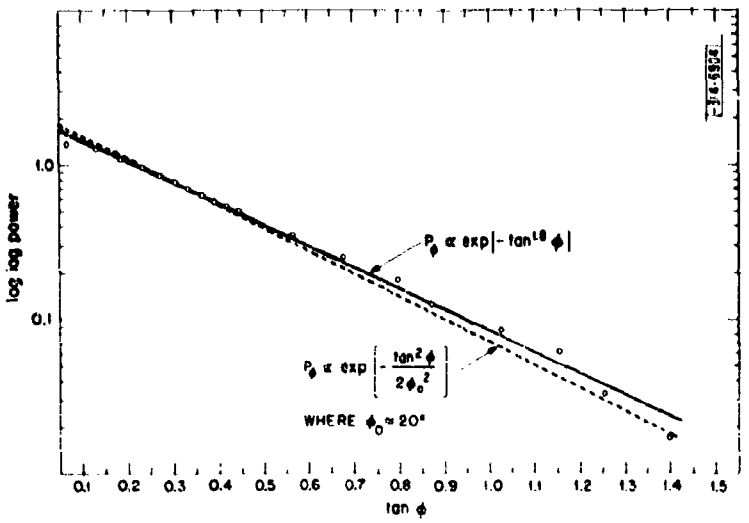

Fig. 28. The "specular" component is here compared with the theoretical law $P(\phi) \propto \exp[-(\tan^2\phi/2\phi_o^2)]$ by plotting log [log power] vs log tan ϕ.

Accordingly the results were plotted for a comparison with this theoretical law (Fig. 28), and a curve

$$P(\varphi) \propto \exp[-\tan^{1.8}\varphi] \tag{13}$$

was found to fit the results closely over the range $6° < \varphi < 55°$. The theoretical curve $P(\varphi) \propto \exp[-\tan^2\varphi/2\varphi_o^2]$ is also shown in Fig. 28, and to within the limits of the experimental error probably fits the points almost as well. Thus the proposed angular power spectrum at 3.6-cm wavelength is

$$P(\varphi) = P_{\varphi=0}\left\{\exp\left[-\frac{\tan^2\varphi}{2\varphi_o^2}\right] + \frac{\cos\varphi}{50}\right\} . \tag{14}$$

The value of φ_o obtained from Fig. 28 is 0.355 radian, or approximately 20.2°.

VI. ACCURACY OF THE MEASUREMENTS

The difference between the two profiles for $\bar{P}(t)$ obtained at wavelengths of 68 and 3.6 cm (Fig. 24) is quite significant. In order to test the validity of these new measurements, an attempt was made to repeat the measurements of Pettengill[15] at 68 cm, using the analogue integration equipment. That is, the detector, video amplifier and integrator were moved from Camp Parks to Millstone Hill and measurements were made with the 440-Mcps radar equipment at a pulse length of 65 μsec. The method of operating the integrator equipment and analyzing the results was precisely the same as for the 3.6-cm measurements, except that no corrections for the antenna pattern were necessary because of the wide beam (2.1°) employed at this frequency. The results of this work are shown in Fig. 29 which is a composite curve for $\bar{P}(t)$ obtained from measurements using 20-, 100- and 500-μsec gate widths.

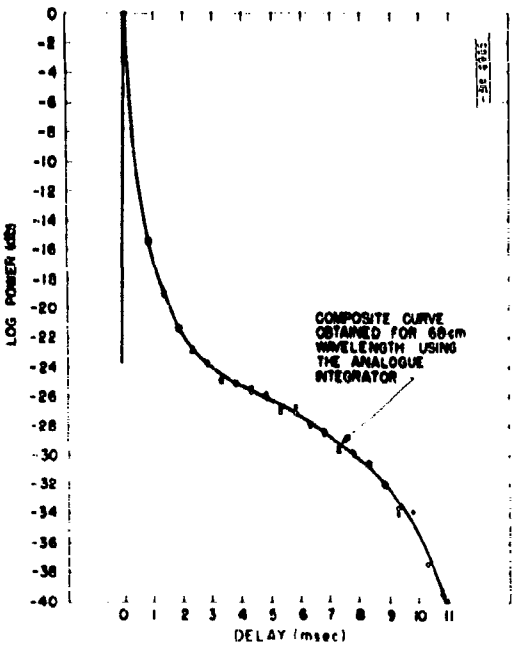

Fig. 29. Echo power as a function of range observed at a wavelength of 68 cm on 10 November 1961, using the integrator equipment described in Sec. II-D to obtain the mean echo intensity. This curve is almost identical with that obtained by Pettengill[15] (Fig. 24) except near the peak. Because the sampling intervals could not be made sufficiently small, Pettengill was unable to resolve the peak fully and his curve rises 1 db less than that shown in the figure.

In Pettengill's measurements the integration process was performed by sampling the echo amplitude and converting the samples to digital numbers. These numbers were then summed and stored in a computer. This particular system has a range resolution of only 400 μsec, and Pettengill was obliged to "interlace" several curves taken when the moon was at slightly different ranges in order to obtain a composite curve with sufficient resolution near the peak. The analogue integrator, on the other hand, was used with a range resolution of 20 μsec. Thus the peak was better defined in these new measurements, and rises 1.3 db above the level observed by Pettengill. Elsewhere the two curves (Figs. 24 and 29) agree to within a few tenths of a decibel over the entire range of delays. It is concluded from this study that the integrator is in no way responsible for the difference between the two curves in Fig. 24.

There are other possible sources of error. They include nonlinearity of the amplifiers in the receiver, but checks were made which exclude this possibility. The results for the central region are very susceptible to inaccuracies in the pointing of the antenna. The digital electronic control system maintained the commanded position within ±0.014° (i.e., ±0.1 beamwidth) of the center of the moon. However, there may have been boresight errors that displaced the true position of the beam from the axis of the antenna which were substantially larger than this. The agreement between the results obtained (Figs. 14, 15) with the antenna displaced from the center of the moon by equal amounts in different directions suggests that any such boresight errors must be small (i.e., $\leq \pm 0.02°$). However, the possibility that the boresight errors are themselves a function of the antenna elevation cannot be excluded as a small source of error in these measurements.

VII. DISCUSSION OF THE RESULTS

Pettengill[15] has shown that, at a 68-cm wavelength, the "rough" component arises from scatterers which cover nine per cent of the surface, if it is assumed that both types of scatterer are composed of the same kind of material. In the present results some 30 per cent of the total power is returned by the "rough" component. We can assume (as Pettengill has done) that the "specular" component is isotropic, i.e., it does not scatter more favorably toward the radar than in any other direction. The "rough" component, on the other hand, will not be isotropic and will exhibit a gain g given by

$$g = \frac{4\pi \int_0^{\pi/2} P(\varphi) \sin\varphi \, d\varphi}{\int_0^{\pi/2} \int_0^{\pi/2} \int_0^{2\pi} P(i\varphi\Theta) \sin i \sin\varphi \, di \, d\varphi \, d\Theta} , \qquad (15)$$

where $P(i\varphi\Theta)$ describes how the power reflected from an element of surface varies with the angles $i\varphi$ and Θ which are specified in Fig. 30. $P(\varphi)$ is the special case where $i = \varphi$ and $\Theta = 0$ and this

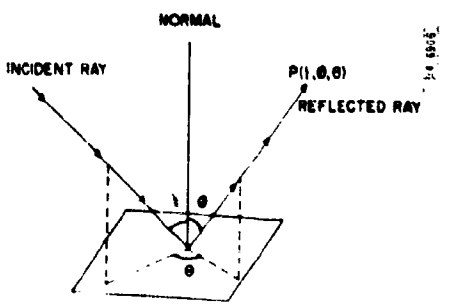

Fig. 30. The surface photometric function $P(i\varphi\theta)$.

is the only case that can be studied by means of radar measurements on the earth. Because the complete function $P(i\varphi\Theta)$ cannot be measured (by earth-based radars alone), we cannot rigorously determine g, the directivity. However, we may obtain an insight into its value by computing g for certain optical laws. For instance, Lambert's law states that

$$P(i\varphi\Theta) \propto \cos i \cos\varphi \tag{16}$$

and has been shown[23] to yield a value g = 2.66. No simple function describes the photometric law $P(i\varphi\Theta)$ for the moon at optical wavelengths.[8] This is unfortunate, because the uniform brightness of the limb region observed in these results suggests that the complete scattering law $P(i\varphi\Theta)$ may be very similar to that obeyed at optical wavelengths. The function

$$P(i\varphi\Theta) \propto \frac{\cos i}{\cos i + \cos\varphi}\,(1 + \cos^2\Theta) \tag{17}$$

provides an approximate fit to the photometric observations of the moon's brightness[8] and if this expression [Eq. (17)] is substituted into the equation for the gain g [Eq. (15)], a value g = 2.68 can be obtained by numerical integration. Thus, if the assumption is made that this value is the appropriate one to take for the gain of the rough component, the fraction of the surface, which must be covered by this type of scatter, can be determined and is 14 per cent.

Hayre and Moore[7] have shown that many kinds of terrain on earth may be described by an autocorrelation function, which defines the correlation between the heights of two points on the surface as a function of their horizontal distance d apart of the form

$$\rho(d) = \exp[-|d|/B] \quad , \tag{18}$$

where B is a characteristic scale of the surface. They have further shown[24] that the angular power spectrum for such surfaces can be obtained as a rather complicated function of φ, the angle of incidence, λ, the radio wavelength, B, the characteristic scale and h_m, the standard deviation of the height fluctuations (assuming these to be normally distributed). The function $\exp[-10.5 \sin\varphi]$ observed by Pettengill[15] approximates to $\exp[-10.5\varphi]$ for small φ, and Hayre[24] claims that this is a special case of his general law for the angular power spectrum. Quite independently Daniels[5] has succeeded in showing that a surface, which can be described by an exponential autocorrelation function, would give rise to an angular power spectrum of the form observed by Pettengill[15] and Hughes.[10] Hayre and Moore[7] speculate that the law $\exp[-|d|/B]$ may hold for smaller height h and distance d intervals than they were able to examine. Because of the finite contour intervals on the maps which these authors examined, structure size of the order of less than 3 cm in height was not included. Thus, though their statement may be true for the earth, it seems unlikely in the case of the moon in view of the photometric evidence, which indicates that the moon is exceedingly rough over small height intervals h and surface distances d. Hence, near the origin, the correlation function $\rho(d)$ probably no longer has an exponential form. The results presented here indicate that the "specular" component obeys the scattering law predicted by Hagfors[21] and Spetner and Katz[22] for a surface having a Gaussian autocorrelation function

$$\rho(d) = \exp\left[-\frac{d^2}{2d_0^2}\right] \tag{19}$$

(where d_0 is the horizontal scale of the undulations), which gives rise to an angular power spectrum

$$P_\varphi = \exp\left[-\frac{\tan^2\varphi}{2\varphi_o^2}\right] \quad , \tag{20}$$

where $\varphi_o = h_m/d_o$ in which h_m is the rms height fluctuation. Thus the average surface gradient is φ_o and the value obtained in these experiments is approximately one in three. This is considerably steeper than the values inferred for longer wavelength measurements[5,6,20] which center around one in ten. It is therefore concluded that, when surface structure on the moon of the order of 0.5 cm is examined, the surface is still largely smooth (only 14 per cent appears rough) but that the average surface gradient is one in three and the autocorrelation function now resembles a Gaussian function more closely than an exponential function.

At first sight it seems surprising that the angular power spectrum $P(\varphi)$ can be the same at 68 (Pettengill[15]) and 10 cm (Hughes[10]), yet different at 3-cm wavelength. It must be borne in mind, however, that the law $P(\varphi) \propto \exp[-10\varphi]$ was observed by Hughes only over the range $3° < \varphi < 14°$. Thus the range of angles common to Pettengill's and Hughes' measurements is $7° < \varphi < 14°$. The measurements reported here have been shown (Fig. 26) to obey a similar exponential-sine law ($\exp[-7 \sin\varphi]$) over the range $6° < \varphi < 18°$ but not beyond. It would be expected that the 10-cm observations should show closer resemblance to the 3.6-cm observations than to those at 68 cm. Hence Hughes might have found that $P(\varphi)$ departed from the law $\exp[-10\varphi]$ for angles $\varphi > 20°$ approximately, had he been able to make measurements at the corresponding time delays. In short, the observations at 10 cm by Hughes do not conflict with the measurements reported here, since they were not made over the same large range of angles of incidence φ.

VIII. CONCLUSIONS

Pulsed-radar measurements at a wavelength of 3.6 cm have been used to determine the brightness distribution over the surface of the moon. The angular power spectrum obtained from this work is

$$P(\varphi) = P_{\varphi=0}\left\{\exp\left[-\frac{\tan^2\varphi}{2\varphi_o^2}\right] + \frac{\cos\varphi}{50}\right\} \quad . \tag{21}$$

The second term closely resembles the behavior of the moon at optical wavelengths, and it is concluded that the scatterers responsible for this form of reflection are distributed over 14 per cent of the surface. The first term is attributed to the smoother portions of the surface (i.e., smoother than approximately ±0.5 cm) which appear to be described by a Gaussian spatial autocorrelation function. These undulations have an average gradient of one in three, which is approximately three times that obtained from observations at meter wavelengths.

The integrated reflected power yields a value for the radar cross section of the moon of 2 per cent of the physical cross section (πa^2). This is substantially lower than the average value obtained at meter wavelengths (7 per cent), and the only previous measurement at 3 cm (9 per cent). However, two published measurements for wavelengths close to 10 cm also indicate a cross section of 2 per cent. It is possible that all three low values result from undetected losses in the radar equipments employed, or that the reflection coefficient is substantially lower at these short wavelengths. This second possibility could well result from the presence of a thin layer of dust overlying most parts of the surface. The existence of such a layer has frequently been postulated to explain the radiometric temperature measurements of the lunar surface. For

communications purposes, the fact that the "specular" returns from the leading edge of the moon are less prominent (approximately 10 db) at 3.6- than at 68-cm wavelength is to be regretted. However, at this frequency it is not difficult to limit the over-all range broadening by employing parabolic antennas of conventional size. In Appendix A, it is shown that the bandwidth of the Project West Ford system (60-foot antennas), using the moon as a reflector, is about ±1 kcps. This is substantially the same as is observed at meter wavelengths.

ACKNOWLEDGMENTS

The author is indebted to W.E. Morrow for kindly permitting the Camp Parks radar equipment to be used for these experiments and for showing considerable interest in their outcome. B. Nichols (also of Group 36) and a band of able technicians operated the equipment in a most efficient manner and were largely responsible for the success of the experiments. W.A. Reid of Group 314 assisted the author in obtaining the data.

Helpful discussions have been held with several members of the staff. These include D. Karp, G.H. Pettengill and R. Price. I am also grateful to L. Niro of Group 315 for making available his antenna pattern measurements (Fig. 8) which were needed in order to convert the results for power vs range delay to the true brightness distribution. Finally, thanks are due to P. Flock of Group 34 who assisted the author considerably in the design and construction of the integrator.

APPENDIX A
THE BANDWIDTH OF THE PROJECT WEST FORD COMMUNICATIONS SYSTEM WITH THE MOON AS A REFLECTOR

The concept of bandwidth for a time-varying network such as that provided by a moon-reflection communication circuit is somewhat different from that employed to describe a passive linear electrical filter. In the case of the moon, the total reflected power is not markedly frequency dependent, i.e., the transfer function is essentially flat over a wide frequency range. Thus the transfer function itself does not describe the useful bandwidth of a radio communications system which uses the moon as a reflector. A discussion of the definition of the system bandwidth, together with measurements of the "bandwidth" by different methods, has been given in two earlier reports.[16,18] Here it need only be said that the most useful definition appears to be provided by the cross-correlation function $\gamma(\Delta f)$ which describes the correlation between the amplitudes of two radio waves at frequencies f_1 and f_2 (where $f_1 - f_2 = \Delta f$). That is, two radio waves simultaneously reflected by the moon will fade, and if their frequency separation Δf is increased to the point where the correlation between their amplitudes has fallen to $1/e$, then Δf is the effective bandwidth. It has also been shown that the function $\gamma(\Delta f)$ is the square of the Fourier cosine transform of the infinite impulse response $\bar{P}(t)$.[18] Hence the uncorrected full-line curve for $\bar{P}(t)$ given in Fig. 7 defines the bandwidth of the communications system (for a single channel) which can be employed by the Project West Ford equipment.

An approximate estimate of what this is can be obtained as follows: A function $\bar{P}(t) = P_{t=0} \exp[-at]$ can be made to fit the results of Fig. 7 quite well over the range $0 < t < 1.0$ msec, if $a = 5750$. Thus $\gamma(\Delta f)$ which is the square of the Fourier cosine transform of this, is given by

$$\gamma(\Delta f) \approx \text{constant} \left[\frac{a}{a^2 + (2\pi\Delta f)^2}\right]^2 . \qquad (A-1)$$

If the constant is chosen to normalize $\gamma(\Delta f) = 1$ for $\Delta f = 0$, then

$$\gamma(\Delta f) \approx \left[\frac{1}{1 + [\frac{\Delta f}{914}]^2}\right]^2 . \qquad (A-2)$$

It follows that the useful single-channel bandwidth of the system is approximately ±1 kcps. This is substantially the same as that found by Ingalls, et al.,[16] at a wavelength of 73 cm, and demonstrates that, although the specular reflections are less predominant over the diffuse component at 3.6 than at 68 cm, for communications purposes this can be offset by narrow antenna beamwidths.

REFERENCES

1. J.V. Evans, "Radio Echo Studies of the Moon," Physics and Astronomy of the Moon, edited by Z. Kopal (Academic Press, New York, 1962). Alternatively, see 3G-0001 [U], Lincoln Laboratory, M.I.T. (30 August 1960).
2. J.V. Evans, "The Scattering Properties of the Lunar Surface at Radio Wavelengths," 3G-0004 [U], Lincoln Laboratory, M.I.T. (10 January 1961), ASTIA 250684, H-248.
3. J.V. Evans and G.H. Pettengill, "The Scattering Properties of the Lunar Surface at Radio Wavelengths," The Solar System, Vol. IV, edited by G.P. Kuiper and B.M. Middlehurst, in press.
4. A.V. Markov, "Brightness Distribution Over the Lunar Disk at Full Moon," Astron. Zhur. 25, 172 (1948).
5. F.B. Daniels, "A Theory of Radar Reflection from the Moon and Planets," J. Geophys. Res. 66, 1781 (1961).
6. J.K. Hargreaves, "Radar Observations of the Lunar Surface," Proc. Phys. Soc. B73, 536, (1959).
7. H.S. Hayre and R.K. Moore, "Theoretical Scattering Coefficient for Near Vertical Incidence from Contour Maps," J. Research Nat'l Bur. Standards 65D, 427 (1961).
8. M. Minnaert, "Photometry of the Moon," The Solar System, Vol. III, edited by G.P. Kuiper and B.M. Middlehurst (University of Chicago Press, Chicago, 1961).
9. N.M. Kobrin, "Radio Echoes from the Moon in the X and S Band," Radiotek. i Electron. 4, 892 (1959).
10. V.A. Hughes, "Roughness of the Moon as a Radar Reflector," Nature 186, 873 (1960). See also, "Radiowave Scattering from the Lunar Surface," Proc. Phys. Soc. (London) 78, 988 (1961).
11. P.G. Mezger and H. Strassl, "The Thermal Radiation of the Moon at 1420 Mc/s," Planet. Space Sci. 1, 213 (1959).
12. P.E. Green, Jr., "Some Future Experiments in Interplanetary Radar Astronomy," G-Report 34-81 [U], Lincoln Laboratory, M.I.T. (May 1959). Alternatively, see "A Summary of Detection Theory Notions in Radar Astronomy Terms," G-Report 34-84 [U], Lincoln Laboratory, M.I.T. (18 January 1960), ASTIA 245698, H-189.
13. J.V. Evans, "Radar Methods of Studying Distant Planetary Surfaces," Proceedings of the NASA-NSF Space Science Symposium, Virginia Polytechnic Institute (1961).
14. P.E. Green, Jr., "Radar Measurement of Target Characteristics," M.I.T. Radar Astronomy Summer Course (1961), in press.
15. G.H. Pettengill and J.C. Henry, "Radar Measurements of the Lunar Surface," Proceedings of the Lunar Symposium (No. 14 on the Moon), IAU, Leningrad (1960).
16. R.P. Ingalls, L.E. Bird and J.W.B. Day, "Bandpass Measurements of a Lunar Reflection Circuit," 33G-0011 [U], Lincoln Laboratory, M.I.T. (26 January 1961), not generally available.
17. J.L. Lawson and G.E. Uhlenbeck, Threshold Signals (McGraw-Hill, New York, 1950), p. 61.
18. J.V. Evans, "Radio Communication Using Moon Reflected Signals," 3G-0003 [U], Lincoln Laboratory, M.I.T. (19 December 1960), ASTIA 249355, H-237. Alternatively, see "The Bandwidth of a Moon Communication Circuit," Brit. J. Appl. Phys. 12, 406 (1961).
19. S.J. Fricker, R.P. Ingalls, W.C. Mason, M.L. Stone and D.W. Swift, "Computation and Measurement of the Fading Rate of Moon-Reflected UHF Signals," J. Research Nat'l Bur. Standards 64D, 455 (1960). Alternatively, see Technical Report No. 187 [U], Lincoln Laboratory, M.I.T. (22 December 1958), ASTIA 204519, H-3.

20. W. K. Victor, R. Stevens and S. W. Golomb, "Radar Exploration of Venus," Technical Report No. 32-132, Jet Propulsion Laboratory, University of California (1961).

21. T. Hagfors, "Some Properties of Radio Waves Reflected from the Moon and their Relation to the Lunar Surface," J. Geophys. Research 66, 777 (1961).

22. L. M. Spetner and L. Katz, "Two Statistical Models for Radar Terrain Return," Trans. IRE, PGAP AP-8, 242 (1960).

23. D. D. Grieg, S. Metzger and R. Waer, "Consideration of Moon-Relay Communication," Proc. IRE 36, 652 (1948).

24. H. S. Hayre, "Radar Scattering Cross Section Applied to Moon Return," Proc. IRE 49, 1433 (1961).

For convenience in ordering copies of Lincoln Laboratory reports cited in this document, each reference is followed by its ASTIA number. In addition, Unclassified (released) reports have also been assigned Hayden serials (designated H-), indicating that they are obtainable, at cost, as microfilm or photoprint copies from the Micro-Reproduction Service, Hayden Memorial Library, M.I.T., Cambridge 39, Massachusetts.